Helsinki University of Technology Institute of Intelligent Power Electronics Publications
Espoo 2003 Publication 7

LOW-FREQUENCY SIGNAL-INJECTION METHOD FOR SPEED SENSORLESS VECTOR CONTROL OF INDUCTION MOTORS

Thesis for the degree of Doctor of Science in Technology

Veli-Matti Leppänen

Dissertation for the degree of Doctor of Science in Technology to be presented with due permission of the Department of Electrical and Communications Engineering for public examination and debate in Auditorium S3 at Helsinki University of Technology (Espoo, Finland) on the 17th of December, 2003, at 12 noon.

Helsinki University of Technology
Department of Electrical and Communications Engineering
Power Electronics Laboratory

Teknillinen korkeakoulu
Sähkö- ja tietoliikennetekniikan osasto
Tehoelektroniikan laboratorio

Distribution:
Helsinki University of Technology
Power Electronics Laboratory
P.O. Box 3000
FIN-02015 HUT
Fax: +358-9-451 2432

ISBN 951-22-6851-5
ISBN 951-22-6842-6 (printed version)
ISSN 1456-0445

Espoo 2003

Abstract

A new method for the speed sensorless vector control of induction motors at low speeds is presented. The method overcomes the well-known low-speed limitations of conventional methods based on an ideal motor model, yet without relying on a more detailed motor model or parasitic effects. To overcome the low-speed limitations, the ideal motor model is augmented with mechanical dynamics. The response of the electromechanical system to a low-frequency ac current signal injected into the stator winding depends on the direction of the signal relative to the rotor flux direction. Based on this dependency, a new algorithm for rotor flux angle estimation, applicable when the total moment of inertia is not too high, is developed. The estimation method tolerates any low-speed operation point, including zero stator frequency, which is validated by simulations and experiments. The robustness of the method against errors in motor parameter estimates is shown both theoretically and experimentally. The algorithm is also combined with a full-order flux observer, yielding fast dynamics in addition to steady-state stability at low speeds.

Keywords: induction motor, sensorless control

Preface

When I decided to continue my studies at the university – after working for several years in industry – I had an idea of concentrating on something already familiar to me, power electronics. To my surprise, Professors Jorma Kyyrä, Jorma Luomi and Seppo Ovaska at the Power Electronics Laboratory managed to turn my mind toward the control of electric drives, something I knew to exist, but did not really understand. Now, four years later, I am deeply grateful to them. After all, the purpose of studying is to learn.

To my advisor, Professor Jorma Luomi, I owe my greatest appreciation. Not only because of the generous help he has given me in scientific and practical matters, but because his attitude and work ethics have made a permanent impression on me.

It has been great fun to work with the other students working at our laboratory, and also to share some spare time with them. Ideas learned from Marko Hinkkanen during our discussions have helped me to keep on track. Discussions with Vesa Tuomainen and Petri Mäki-Ontto have also helped me, often with a lot of laughter.

The staff at the Power Electronics Laboratory has always been available when needed. Thanks belong to our secretary Anja Meuronen for her cheerful attitude when handling the sometimes-dull paper work I had problems with. I had already had the pleasure of working with our laboratory technician Ilkka Hanhivaara on several occasions during the previous three decades. And there was always someone to trouble-shoot my computer!

The financial support given to me by the Graduate School of Electrical Engineering, the Association of Electrical Engineers in Finland, the Finnish Society of Electronics Engineers, Ulla Tuomisen Säätiö and Tekniikan Edistämissäätiö is gratefully acknowledged.

Finally, I thank my wife Mari and our children Ella and Kalle for providing me with a loving home and everything else that I needed while completing my research.

Otaniemi, December 2003
Veli-Matti Leppänen

Contents

List of Publications

This thesis consists of an overview and the following publications:

[P1] V.-M. Leppänen and J. Luomi (2001). Estimating the back-EMF of an induction motor. *Proceedings of the 9th European Conference on Power Electronics and Applications, EPE 2001*, Graz, Austria, 27-29 August, 2001, on CD-ROM.

[P2] V.-M. Leppänen and J. Luomi (2002). Effect of equation of motion on low-frequency impedance of induction motors – an approach for rotor flux angle estimation. *Proceedings of EPE-PEMC 2002*, Cavtat, Croatia, 9-11 September, 2002, on CD-ROM.

[P3] V.-M. Leppänen and J. Luomi (2002). A tracking controller for a speed sensorless induction machine drive. *Proceedings of 2002 Nordic Workshop on Power and Industrial Electronics*, *NORPIE 2002,* Stockholm, Sweden, 12-14 August, 2002, on CD-ROM.

[P4] V.-M. Leppänen and J. Luomi (2002). Rotor flux angle tracking controller for sensorless induction motor drives. *Conference Record of the 2002 IEEE Industry Applications Conference*, *IAS 2002,* Pittsburgh, PA, 13-18 October, 2002, Vol. 2, pp. 856-863.

[P5] V.-M. Leppänen and J. Luomi (2002). Speed sensorless induction machine control for zero speed and frequency. *Conference Record of the 28th Annual Conference of the IEEE Industrial Electronics Society*, *IECON'02*, Sevilla, Spain, 5-8 November, 2002, pp. 400-405.

[P6] V.-M. Leppänen and J. Luomi (2003). Observer using low-frequency injection for sensorless induction motor control - parameter sensitivity analysis. *Conference Record of the IEEE International Electric Machines and Drives Conference*, *IEMDC 2003,* Madison, WI, 1-4 June, 2003, pp. 609-616.

[P7] V.-M. Leppänen (2003). Low-frequency injection-based speed sensorless control of induction motors – applicability and implementation aspects. *Proceedings of the 10th European Conference on Power Electronics and Applications*, *EPE 2003,* Toulouse, France, 2-4 September, 2003, on CD-ROM.

[P8] M. Hinkkanen, V.-M. Leppänen, and J. Luomi (2003). Flux observer enhanced with low-frequency signal injection allowing sensorless zero-frequency operation of induction motors. *Conference Record of the 2003 IEEE Industry Applications Conference*, *IAS 2003,* Salt Lake City, UT, 12-16 October, 2003, pp. 1150-1156.

[P9] T. Kereszty, V.-M. Leppänen, and J. Luomi (2003). Sensorless control of surface magnet synchronous motors at low speeds using low-frequency signal injection. *Conference Record of the 29th Annual Conference of the IEEE Industrial Electronics Society*, *IECON'03,* Roanoke, VA, 2-6 November, 2003, pp. 1239-1243.

The author has written Publications [P1] – [P7] with help and guidance from Professor Luomi in refining the texts. Professor Luomi suggested the use of impedances in Publication [P2] to describe the response of the electromechanical system to the test signal. He also suggested the analysis of the applicability of the method in terms of the total moment of inertia in the system in Publications [P2] and [P7].

Publication [P8] was written mainly by M. Hinkkanen. The author wrote the parts introducing and describing the signal-injection method. The actual combination of the speed-adaptive full-order flux observer and the signal-injection method was achieved by M. Hinkkanen, who also made the simulations and experiments. The author contributed to his work only through discussion and comments, except for helping refine the final text.

Publication [P9] was jointly written by all three writers. The author contributed the basic idea of applying the signal-injection method to even surface magnet synchronous motors, and helped T. Kereszty in building the simulation model.

In addition to the publications, the author has contributed to the development and maintenance of the experimental laboratory setup used in the experiments.

Symbols

b	coefficient of viscous friction
$\hat{b}$	estimate of the coefficient of viscous friction
$\underline{e}$	back-emf space vector in the rotor flux reference frame
$\underline{e}^{\mathrm{k}}$	back-emf space vector in an arbitrary reference frame
$\underline{e}^{\mathrm{s}}$	back-emf space vector in the stationary reference frame
e_{cq}	response of the q component of the back-emf to the test signal in the rotor flux reference frame
$e_{\mathrm{cq}}^{\varepsilon}$	response of the q component of the back-emf to the test signal in the estimated rotor flux reference frame
F_{ε}	error signal
$i_{\mathrm{a}},\ i_{\mathrm{b}},\ i_{\mathrm{c}}$	phase currents
i_{cd}	ac current test signal
$i_{\mathrm{cd}}^{\varepsilon},\ i_{\mathrm{cq}}^{\varepsilon}$	current signals in d and q directions in the controller's reference frame
$i_{\mathrm{d}},\ i_{\mathrm{q}}$	real and imaginary parts of $\underline{i}_{\mathrm{s}}$
i_{d0}	quiescent value of flux-producing stator current component
i_{q0}	quiescent value of torque-producing stator current component
i_{M}	magnitude of the magnetizing current space vector of the Γ-equivalent circuit
$\underline{i}_{\mathrm{M}}^{\mathrm{s}}$	magnetizing current space vector of the Γ-equivalent circuit in the stationary reference frame
$\underline{i}_{\mathrm{m}}^{\mathrm{s}}$	magnetizing current space vector of the T-equivalent circuit in the stationary reference frame
$\underline{i}_{\mathrm{R}}^{\mathrm{s}}$	rotor current space vector of the Γ-equivalent circuit in the stationary reference frame
$\underline{i}_{\mathrm{r}}^{\mathrm{s}}$	rotor current space vector of the T-equivalent circuit in the stationary reference frame

i_{Rq}	imaginary part of rotor current space vector of the Γ-equivalent circuit in the rotor flux reference frame
$\underline{i}_{\mathrm{s}}$	stator current space vector in the rotor flux reference frame
$\underline{i}_{\mathrm{s}}^{\mathrm{k}}$	stator current space vector in an arbitrary reference frame
$\underline{i}_{\mathrm{s}}^{\mathrm{s}}$	stator current space vector in the stationary reference frame
J	moment of inertia
$\hat{J}$	estimate of the moment of inertia
j	imaginary unit related to the space vectors
L_{M}	magnetizing inductance in the Γ-equivalent circuit
L_{m}	magnetizing inductance in the T-equivalent circuit
L_{σ}	total leakage inductance
$L_{\sigma\mathrm{r}}$	rotor leakage inductance
$L_{\sigma\mathrm{s}}$	stator leakage inductance
p	number of pole pairs
R_{R}	rotor resistance in the Γ-equivalent circuit
R_{r}	rotor resistance in the T-equivalent circuit
R_{s}	stator resistance
s	Laplace-variable
t	time
T^{ref}	reference value for load torque
T_{act}	measured shaft torque
T_{e}	electromagnetic torque
T_{ec}	response of the electromagnetic torque T_{e} to the test signal
T_{L}	load torque
u_{dc}	dc link voltage of a frequency converter
$\underline{u}_{\mathrm{s}}$	stator voltage space vector in the rotor flux reference frame
$\underline{u}_{\mathrm{s}}^{\mathrm{k}}$	stator voltage space vector in an arbitrary reference frame
$\underline{u}_{\mathrm{s}}^{\mathrm{s}}$	stator voltage space vector in the stationary reference frame
$\underline{x}^{\mathrm{s}}$	space vector of the phase quantities $x_{\mathrm{a}},\ x_{\mathrm{b}},\ x_{\mathrm{c}}$, expressed in the stationary reference frame
$x_{\mathrm{a}},\ x_{\mathrm{b}},\ x_{\mathrm{c}}$	general phase quantities
$x_{\alpha},\ x_{\beta}$	real and imaginary parts of $\underline{x}^{\mathrm{s}}$

ε	error of the rotor flux angle estimation
θ_1	rotor flux angle
$\hat{\theta}_1$	estimated rotor flux angle
τ_r	rotor time constant
$\hat{\tau}_\mathrm{r}$	estimate of the rotor time constant
ψ	flux linkage
$\underline{\psi}$	space vector of ψ
ψ_R	magnitude of the rotor flux linkage space vector of the Γ-equivalent circuit
$\underline{\psi}_\mathrm{R}$	rotor flux linkage space vector of the Γ-equivalent circuit in the rotor flux reference frame
$\underline{\psi}_\mathrm{R}^\mathrm{k}$	rotor flux linkage space vector of the Γ-equivalent circuit in an arbitrary reference frame
$\underline{\psi}_\mathrm{R}^{\mathrm{k}*}$	complex conjugate of $\underline{\psi}_\mathrm{R}^\mathrm{k}$
$\underline{\psi}_\mathrm{R}^\mathrm{s}$	rotor flux linkage space vector of the Γ-equivalent circuit in the stationary reference frame
$\psi_\mathrm{Rd}^\mathrm{k}$, $\psi_\mathrm{Rq}^\mathrm{k}$	real and imaginary parts of $\underline{\psi}_\mathrm{R}^\mathrm{k}$
$\underline{\psi}_\mathrm{r}^\mathrm{s}$	rotor flux linkage space vector of the T-equivalent circuit in the stationary reference frame
ω_1	angular frequency of rotor flux linkage space vector in electrical radians per second
ω_2	slip angular frequency in electrical radians per second
ω_c	angular frequency of the ac current test signal
ω_k	angular speed of an arbitrary reference frame in electrical radians per second
ω_m	angular speed of the shaft in electrical radians per second
$\omega_\mathrm{m}^\mathrm{ref}$	reference value for ω_m
ω_mc	response of the angular speed ω_m to the test signal

1 Introduction

The three-phase cage induction motor is the most popular electric motor type used in industry and by utilities. Its popularity stems from several factors: ruggedness and simplicity of construction make the induction motor a reliable, long-lived, easy-to-maintain and low-cost solution, while its ability to start and operate directly from the grid without any extra hardware is unique. Energy-efficient speed control of the induction motor is possible by adjusting the frequency of the supply voltage, which is usually done by means of a frequency converter. In the most common type of frequency converter, the line voltage is first rectified into dc voltage, which is subsequently inverted into an adjustable ac voltage using Pulse-Width-Modulation (PWM) techniques.

The control strategies of the inverter-motor combination may be classified into two broad categories: open-loop *scalar control* strategies for applications with moderate static and dynamic performance requirements, and closed-loop *vector control* strategies for high-performance applications. In vector control, the flux linkage magnitude and the electromagnetic torque are controlled independently of each other, by analogy with the dc machine. The independent control is made possible by dividing the stator current vector into components parallel and perpendicular to the flux linkage vector, i.e., into flux-producing and torque-producing components. The division can be made only if the direction of the flux linkage vector is known, as demonstrated by Blaschke, who is credited for his pioneering work in the vector control of induction motors (Blaschke 1972). Usually it is either the stator flux linkage or the rotor flux linkage that is selected for control.

The key to vector control is thus the correct observation of the orientation of the flux linkage (which is often called the *field orientation*) and, thereafter, the independent control of the mutually perpendicular stator current components. However, if there is an error in the orientation, a cross-coupling between the flux and torque control leads to poor dynamic performance and may increase the power losses in the motor. Moreover, a flux level considerably lower than desired may cause the motor to lose the required torque-producing capability. The field orientation is

relatively straightforward in all operating conditions if the angular speed of the rotor is accurately known, which traditionally necessitates a sensor on the shaft of the motor. However, there are several reasons for preferring a system without the sensor. The sensor and its signal cable, together with the installation work, are costly. The hardware also occupies extra space and reduces the reliability of the system. In low-power applications, the extra cost and space requirements are substantial relative to those of the motor and frequency converter alone. Moreover, it may be impossible to have a sensor in a hostile environment.

The speed sensorless vector control of induction motors has been the subject of increasingly keen research during the last two decades (Rajashekara et al. 1996, Holtz 2002). In the context of this thesis, the (speed or position) *sensorless* control means that the only measurements for obtaining the flux orientation are those of the stator current and stator voltage. In practice, estimates of the current, and especially of the voltage, are often obtained from other readily available signals within the inverter. The problem of sensorless field orientation is very difficult at low speeds, when the stator frequency approaches zero. In part, the difficulty is practical: unfavorable signal-to-noise conditions caused by measurement errors, and errors in motor parameter estimates, deteriorate the flux estimate. There is also a theoretical limitation at zero stator frequency. The fundamental components of the stator current and voltage are pure dc quantities at zero stator frequency, and, if the control is based on the commonly used ideal motor model with sinusoidal air-gap field distribution, it is impossible to estimate the speed of the shaft or the orientation of the rotor flux from these dc quantities (Holtz 2002).

Flux observers exploiting non-ideal characteristics of the induction motor have been developed to circumvent the problem of zero-frequency operation. These observers abandon the ideal motor model in favor of a more detailed one. Usually, the observers excite the stator winding with a high-frequency voltage or current (about 500 Hz), and the response conveys information about the spatial location of a maximum or minimum of the leakage inductance or rotor resistance. The high-frequency excitation may be specifically added to the stator voltage or current; otherwise, the switching harmonics of the inverter may constitute the excitation. The variation of the inductance or resistance along the air-gap periphery can be purposefully designed into the rotor. Alternatively, the observed change in the inductance may be caused by variation in the local saturation. The problem with these signal-injection methods is that they are specific to the motor design and, in most cases, the operating point of the motor affects the interpretation of the response.

An assumption of constant rotor speed is often made in order to simplify the analysis of the flux dynamics of an induction motor. The constant-speed assumption linearizes the otherwise non-linear system. It is reasoned that the currents of a winding can change almost instantaneously, while the acceleration is limited by the moment of inertia in the system. The mechanical dynamics are thus excluded from the treatment of the flux dynamics, and the speed merely enters the voltage equations of the motor as a disturbance. However, the moment of inertia in the system is not always large enough to justify the assumption of constant speed. In fact, if nominal torque is applied and the moment of inertia of the rotor alone is considered, a typical induction motor accelerates from zero to nominal speed in a time interval comparable to the rotor time constant. In such an extreme case, there is no justification for a two-time-scale approach to separate the flux dynamics from the mechanical dynamics.

The research presented in this thesis is motivated by the difficulty of achieving speed sensorless vector control of an induction motor when the stator frequency is close to zero. The target is to develop such a vector control, with the following attributes:

1. There is no speed sensor in the system.
2. The control is based on known stator currents and stator voltage.
3. At low speeds, the system is stable in steady state, under all load torque conditions up to rated torque, in all four quadrants, including zero frequency and zero speed.
4. The system is adequately robust against errors in motor parameter estimates for a practical application.
5. The dynamic performance of the system is comparable to that of speed-sensored vector control.
6. The system is widely applicable with respect to motor size, design, and application.
7. The system is easy to implement.

Since sensorless zero-frequency vector control of an induction motor cannot be achieved by using pure dc quantities, some kind of signal-injection method should be considered. However, the control should preferably rely on a simple, generally applicable motor model.

The work presented in this thesis is based on the ideal motor model, which is augmented with the equation of motion in order to take the mechanical dynamics into account. In addition, a fast stator current control, which removes the dynamics

of the stator winding from the dynamics of the rest of the electromechanical system, is assumed. Thus, the stator voltage is considered to be an output of the current-fed motor. Adding a low-frequency ac current signal (about 25 Hz) to the stator current creates a specific response from the electromechanical system that can be extracted from the stator voltage. The phenomenon is analyzed in this thesis, and it is shown that the response conveys information about the rotor flux direction, provided that the total moment of inertia is not too high. Based on the result, a method for determining the direction of the rotor flux in a speed sensorless induction motor drive is developed. Experimental results indicate that the method is capable of tracking the rotor flux direction in all low-speed operating conditions, including zero frequency. The method is also shown to be insensitive to errors in motor parameter estimates.

2 System Model

2.1 Fundamental-wave motor model

Early work introducing the two-reaction theory (Park 1929) for synchronous generators laid down general principles for the analysis of ac machines. Stanley (1938) proposes its use for the dynamic analysis of induction motors, deriving the induction motor model and solving example problems based on it. The following assumptions were listed by Stanley:

> "1. Balanced rotor windings are assumed for all cases, and the three-phase machine equations are derived upon the additional assumption that the stator windings are also balanced.
> 2. It is assumed that the coefficient of mutual inductance between any stator winding and any rotor winding is a cosinusoidal function of the electrical angle between the axes of the two windings.
> 3. It is further assumed that the rotor is smooth and that the self-inductances of all the windings are independent of the rotor position.
> 4. The effects of saturation, hysteresis and eddy currents are neglected."

The assumptions yield the constant-parameter, *fundamental-wave model,* for a three-phase induction motor. The assumptions guarantee that the spatial distribution of the air gap field in the motor is always sinusoidal, even if the timely behavior of the currents in the individual windings were not. Thus the fundamental-wave model is also applicable in dynamic analysis. For a similar treatment, see, for example, Kazmierkowski and Tunia (1994).

Space vectors provide an efficient and convenient tool for the analysis of three-phase systems. They were originally developed by Kovács and Rácz (1959). The space vector representing the three phase quantities x_a, x_b, and x_c is a complex quantity $\underline{x}^\mathrm{s}$ defined by

$$\underline{x}^{\mathrm{s}} = \frac{2}{3}\Big(x_{\mathrm{a}} + \mathrm{e}^{\mathrm{j}2\pi/3}x_{\mathrm{b}} + \mathrm{e}^{\mathrm{j}4\pi/3}x_{\mathrm{c}}\Big), \tag{2.1}$$

where the phase quantities may vary arbitrarily in time. The scaling factor 2/3 in (2.1) is chosen so that, if x_{a}, x_{b}, and x_{c} form a symmetrical three-phase system, the magnitude of $\underline{x}^{\mathrm{s}}$ equals the amplitude of the sinusoidal phase quantities. The superscript 's' indicates that the space vector is expressed in the *stationary* reference frame, the real axis of which is attached to the magnetic axis of phase a. The space vector can be expressed by its real and imaginary parts as $\underline{x}^{\mathrm{s}} = x_{\alpha} + \mathrm{j}x_{\beta}$. The reference frame is often chosen differently by attaching its real axis to the space vector of a suitable quantity in the motor, usually the space vector $\underline{\psi}$ of a flux linkage. In this reference frame, the flux linkage $\underline{\psi}$ reduces to a real quantity ψ. Moreover, the steady-state space vectors of the electrical quantities are constant in this reference frame.

The fundamental-wave model of the three-phase induction motor is fully determined by five parameters in the commonly used T-equivalent circuit of the motor: the magnetizing inductance L_{m}, the leakage inductances $L_{\sigma\mathrm{s}}$ and $L_{\sigma\mathrm{r}}$ of the stator and rotor windings, respectively, and the resistances R_{s} and R_{r} of the windings. The dynamic T-equivalent circuit of the induction motor in Fig. 2.1 is given in the stationary reference frame. The variables are the stator voltage $\underline{u}_{\mathrm{s}}^{\mathrm{s}}$, the stator current $\underline{i}_{\mathrm{s}}^{\mathrm{s}}$, the magnetizing current $\underline{i}_{\mathrm{m}}^{\mathrm{s}}$, the rotor current $\underline{i}_{\mathrm{r}}^{\mathrm{s}}$, the rotor flux linkage $\underline{\psi}_{\mathrm{r}}^{\mathrm{s}}$ and the angular speed ω_{m} of the shaft in electrical radians per second.

In this thesis, the dynamic Γ-equivalent circuit is adopted, with all leakage referred to the stator side (De Doncker and Novotny, 1994). The circuit, expressed in the stationary reference frame in Fig. 2.2, is fully determined by only four parameters: the magnetizing inductance L_{M}, the total leakage inductance L_{σ}, the stator resistance R_{s} and the rotor resistance R_{R}.

The relationships between the quantities that are different from each other in the T- and Γ-equivalent circuits are summarized in Table 2.1. The equations governing the Γ-equivalent circuit are the voltage equations for the stator and rotor

$$\underline{u}_{\mathrm{s}}^{\mathrm{s}} = R_{\mathrm{s}}\underline{i}_{\mathrm{s}}^{\mathrm{s}} + L_{\sigma}\frac{\mathrm{d}}{\mathrm{d}t}\underline{i}_{\mathrm{s}}^{\mathrm{s}} + L_{\mathrm{M}}\frac{\mathrm{d}}{\mathrm{d}t}\underline{i}_{\mathrm{M}}^{\mathrm{s}} \tag{2.2}$$

$$0 = R_{\mathrm{R}}\underline{i}_{\mathrm{R}}^{\mathrm{s}} + L_{\mathrm{M}}\frac{\mathrm{d}}{\mathrm{d}t}\underline{i}_{\mathrm{M}}^{\mathrm{s}} - \mathrm{j}\omega_{\mathrm{m}}\underline{\psi}_{\mathrm{R}}^{\mathrm{s}} \tag{2.3}$$

and the flux equations of the stator and rotor

$$\underline{\psi}_{\mathrm{s}}^{\mathrm{s}} = L_{\sigma}\underline{i}_{\mathrm{s}}^{\mathrm{s}} + L_{\mathrm{M}}\underline{i}_{\mathrm{M}}^{\mathrm{s}} \tag{2.4}$$

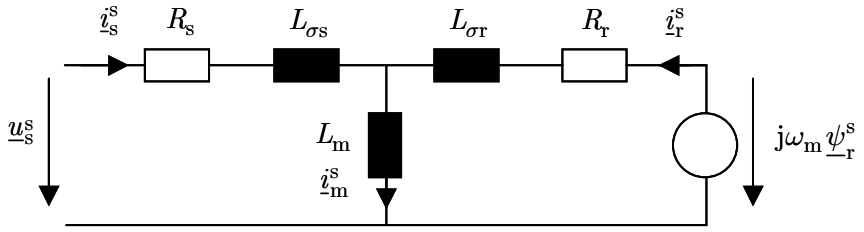

Fig. 2.1. The dynamic T-equivalent circuit of a cage induction motor.

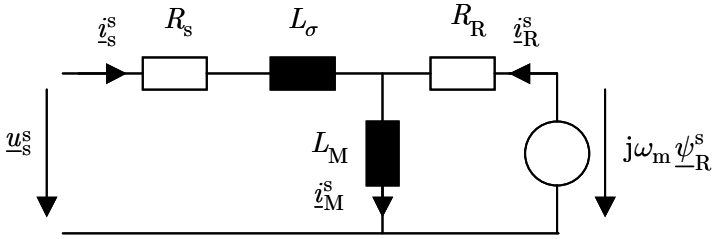

Fig. 2.2. The dynamic Γ-equivalent circuit of a cage induction motor, with all leakage on the stator side.

TABLE 2.1. RELATIONSHIPS BETWEEN THE EQUIVALENT CIRCUITS.

Quantity	T-equivalent circuit	Γ-equivalent circuit
Rotor current	$\underline{i}_\mathrm{r}^\mathrm{s}$	$\underline{i}_\mathrm{R}^\mathrm{s} = \dfrac{L_\mathrm{m}+L_{\sigma\mathrm{r}}}{L_\mathrm{m}}\,\underline{i}_\mathrm{r}^\mathrm{s}$
Rotor flux linkage	$\underline{\psi}_\mathrm{r}^\mathrm{s}$	$\underline{\psi}_\mathrm{R}^\mathrm{s} = \dfrac{L_\mathrm{m}}{L_\mathrm{m}+L_{\sigma\mathrm{r}}}\,\underline{\psi}_\mathrm{r}^\mathrm{s}$
Magnetizing current	$\underline{i}_\mathrm{m}^\mathrm{s}$	$\underline{i}_\mathrm{M}^\mathrm{s} = \underline{i}_\mathrm{s}^\mathrm{s} + \underline{i}_\mathrm{R}^\mathrm{s}$
Rotor resistance	R_r	$R_\mathrm{R} = \left(\dfrac{L_\mathrm{m}}{L_\mathrm{m}+L_{\sigma\mathrm{r}}}\right)^2 R_\mathrm{r}$
Magnetizing inductance	L_m	$L_\mathrm{M} = \dfrac{L_\mathrm{m}^2}{L_\mathrm{m}+L_{\sigma\mathrm{r}}}$
Leakage inductance	$L_{\sigma\mathrm{s}},\ L_{\sigma\mathrm{r}}$	$L_\sigma = L_{\sigma\mathrm{s}} + \dfrac{L_\mathrm{m}L_{\sigma\mathrm{r}}}{L_\mathrm{m}+L_{\sigma\mathrm{r}}}$

$$\underline{\psi}_\mathrm{R}^\mathrm{s} = L_\mathrm{M}\underline{i}_\mathrm{M}^\mathrm{s}\,. \tag{2.5}$$

Eliminating the rotor current $\underline{i}_\mathrm{R}^\mathrm{s} = \underline{\psi}_\mathrm{R}^\mathrm{s}\,/\,L_\mathrm{M} - \underline{i}_\mathrm{s}^\mathrm{s}$ yields the voltage equations with the stator current and rotor flux linkage as state variables

$$L_\sigma\,\frac{\mathrm{d}}{\mathrm{d}t}\,\underline{i}_\mathrm{s}^\mathrm{s} = \underline{u}_\mathrm{s}^\mathrm{s} - (R_\mathrm{s}+R_\mathrm{R})\underline{i}_\mathrm{s}^\mathrm{s} + (R_\mathrm{R}\,/\,L_\mathrm{M} - \mathrm{j}\omega_\mathrm{m})\underline{\psi}_\mathrm{R}^\mathrm{s} \tag{2.6}$$

$$\frac{\mathrm{d}}{\mathrm{d}t}\underline{\psi}_{\mathrm{R}}^{\mathrm{s}} = R_{\mathrm{R}}\underline{i}_{\mathrm{s}}^{\mathrm{s}} - (R_{\mathrm{R}} / L_{\mathrm{M}} - \mathrm{j}\omega_{\mathrm{m}})\underline{\psi}_{\mathrm{R}}^{\mathrm{s}}\,. \tag{2.7}$$

Defining the *back-emf* as

$$\underline{e}^{\mathrm{s}} = (R_{\mathrm{R}} / L_{\mathrm{M}} - \mathrm{j}\omega_{\mathrm{m}})\underline{\psi}_{\mathrm{R}}^{\mathrm{s}} \tag{2.8}$$

simplifies (2.6) and (2.7) to

$$L_\sigma \frac{\mathrm{d}}{\mathrm{d}t}\underline{i}_{\mathrm{s}}^{\mathrm{s}} = \underline{u}_{\mathrm{s}}^{\mathrm{s}} - (R_{\mathrm{s}} + R_{\mathrm{R}})\underline{i}_{\mathrm{s}}^{\mathrm{s}} + \underline{e}^{\mathrm{s}} \tag{2.9}$$

$$\frac{\mathrm{d}}{\mathrm{d}t}\underline{\psi}_{\mathrm{R}}^{\mathrm{s}} = R_{\mathrm{R}}\underline{i}_{\mathrm{s}}^{\mathrm{s}} - \underline{e}^{\mathrm{s}}\,. \tag{2.10}$$

On the other hand, combining (2.2) and (2.5) gives

$$\frac{\mathrm{d}}{\mathrm{d}t}\underline{\psi}_{\mathrm{R}}^{\mathrm{s}} = \underline{u}_{\mathrm{s}}^{\mathrm{s}} - R_{\mathrm{s}}\underline{i}_{\mathrm{s}}^{\mathrm{s}} - L_\sigma \frac{\mathrm{d}}{\mathrm{d}t}\underline{i}_{\mathrm{s}}^{\mathrm{s}}\,, \tag{2.11}$$

which is often used for open-loop estimation of the rotor flux linkage. Equation (2.11) is commonly known as the *voltage model*. Equation (2.7) can also be used for estimating the rotor flux linkage; this is known as the *current model*.

According to (2.8), the back-emf depends only on the speed and rotor flux linkage, while its component perpendicular to the flux linkage carries information about the speed (irrespective of the reference frame where the equations are written). If the stator current is forced into the motor arbitrarily, then, according to (2.9), the stator voltage must adapt itself to the constraints set by the back-emf and the stator current. This is illustrated in Fig. 2.3, where the stator current can be considered the known input, the back-emf the unknown input, and the stator voltage the output. It is clear that the back-emf can be solved from the known stator quantities, provided that the motor parameters are known.

Equations (2.8) - (2.10) can be transformed to an arbitrary reference frame rotating at angular frequency ω_{k}:

$$\underline{e}^{\mathrm{k}} = (R_{\mathrm{R}} / L_{\mathrm{M}} - \mathrm{j}\omega_{\mathrm{m}})\underline{\psi}_{\mathrm{R}}^{\mathrm{k}} \tag{2.12}$$

$$L_\sigma \frac{\mathrm{d}}{\mathrm{d}t}\underline{i}_{\mathrm{s}}^{\mathrm{k}} = \underline{u}_{\mathrm{s}}^{\mathrm{k}} - (R_{\mathrm{s}} + R_{\mathrm{R}})\underline{i}_{\mathrm{s}}^{\mathrm{k}} - \mathrm{j}\omega_{\mathrm{k}} L_\sigma \underline{i}_{\mathrm{s}}^{\mathrm{k}} + \underline{e}^{\mathrm{k}} \tag{2.13}$$

$$\frac{\mathrm{d}}{\mathrm{d}t}\underline{\psi}_{\mathrm{R}}^{\mathrm{k}} = R_{\mathrm{R}}\underline{i}_{\mathrm{s}}^{\mathrm{k}} - \mathrm{j}\omega_{\mathrm{k}}\underline{\psi}_{\mathrm{R}}^{\mathrm{k}} - \underline{e}^{\mathrm{k}}\,. \tag{2.14}$$

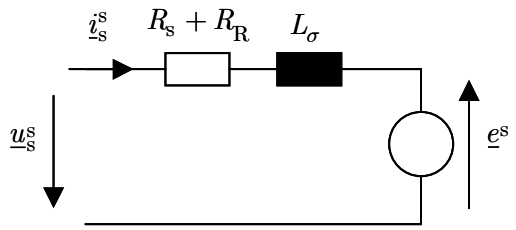

Fig. 2.3. Circuit of an induction motor relating the stator variables to the back-emf.

When the reference frame is attached to the rotor flux, rotating at angular frequency ω_1, the equations become

$$\underline{e} = (R_\mathrm{R} / L_\mathrm{M} - \mathrm{j}\omega_\mathrm{m})\psi_\mathrm{R} \tag{2.15}$$

$$L_\sigma \frac{\mathrm{d}}{\mathrm{d}t}\underline{i}_\mathrm{s} = \underline{u}_\mathrm{s} - (R_\mathrm{s}+R_\mathrm{R})\underline{i}_\mathrm{s} - \mathrm{j}\omega_1 L_\sigma \underline{i}_\mathrm{s} + \underline{e} \tag{2.16}$$

$$\frac{\mathrm{d}}{\mathrm{d}t}\psi_\mathrm{R} = R_\mathrm{R}\underline{i}_\mathrm{s} - \mathrm{j}\omega_1\psi_\mathrm{R} - \underline{e}\,. \tag{2.17}$$

Writing the stator current as $\underline{i}_\mathrm{s} = i_\mathrm{d} + \mathrm{j}i_\mathrm{q}$ and realizing that in the rotor flux reference frame $\underline{\psi}_\mathrm{R} = \psi_\mathrm{R} + \mathrm{j}0$, (2.15) and (2.17) can be combined and split into real and imaginary parts:

$$\frac{\mathrm{d}}{\mathrm{d}t}\psi_\mathrm{R} = R_\mathrm{R} i_\mathrm{d} - \frac{R_\mathrm{R}}{L_\mathrm{M}}\psi_\mathrm{R} \tag{2.18}$$

$$0 = R_\mathrm{R} i_\mathrm{q} - (\omega_1 - \omega_\mathrm{m})\psi_\mathrm{R}\,. \tag{2.19}$$

According to (2.18), the rotor flux linkage magnitude ψ_R can be controlled by adjusting the stator current component i_d. In steady state, the derivative is zero and (2.18) gives $i_\mathrm{d} = \psi_\mathrm{R} / L_\mathrm{M}$. Hence there is no rotor current in the d direction and the magnetization comes exclusively from the stator current d component: $\underline{i}_\mathrm{M} = i_\mathrm{d}$.

Equation (2.19) can be rearranged as

$$\omega_2 = R_\mathrm{R} i_\mathrm{q} / \psi_\mathrm{R}\,, \tag{2.20}$$

where the slip angular frequency $\omega_2 = \omega_1 - \omega_\mathrm{m}$ has been introduced. Equation (2.20) is known as the *slip relation*. A steady-state form of the slip relation often used is $\omega_2\tau_\mathrm{r} = i_\mathrm{q} / i_\mathrm{d}$, where $\tau_\mathrm{r} = L_\mathrm{M} / R_\mathrm{R}$ is the rotor time constant. In the rotor flux reference frame, $i_\mathrm{q} = -i_\mathrm{Rq}$ always.

The electromagnetic torque can be expressed as

$$T_\mathrm{e} = \frac{3p}{2}\mathrm{Im}\left\{\underline{\psi}_\mathrm{R}^{\mathrm{k}*}\underline{i}_\mathrm{s}^\mathrm{k}\right\}, \tag{2.21}$$

where p is the number of pole pairs, and $\underline{\psi}_\mathrm{R}^{\mathrm{k}*} = \psi_\mathrm{Rd}^\mathrm{k} - \mathrm{j}\psi_\mathrm{Rq}^\mathrm{k}$ is the complex conjugate of the rotor flux linkage vector in the arbitrary reference frame. The torque is

independent of the reference frame selected; in the rotor flux reference frame, the expression of torque becomes particularly simple:

$$T_\mathrm{e} = \frac{3p}{2}\psi_\mathrm{R} i_\mathrm{q}\,. \tag{2.22}$$

2.2 Observability of the rotor flux or speed

Flux observers based on the fundamental-wave motor model can be used if the frequency is high enough. If the stator frequency differs from zero, and if the parameters are exactly known, then it is, in principle, possible to observe the rotor flux from the stator current and voltage in steady state, a fact that becomes evident from the steady-state space vector diagram in Fig. 2.4. The diagram is based on the fundamental-wave motor model, and is obtained from (2.15) - (2.17) by setting the time derivatives to zero. The q axis is found by subtracting the voltage drops of the total leakage inductance and the stator resistance from the stator voltage. Hence, the direction of the rotor flux (d axis) is also known. The magnitude of the rotor flux is found as the product of the magnetizing inductance and the d component of the stator current: $\psi_\mathrm{R} = L_\mathrm{M} i_\mathrm{d}\,.$

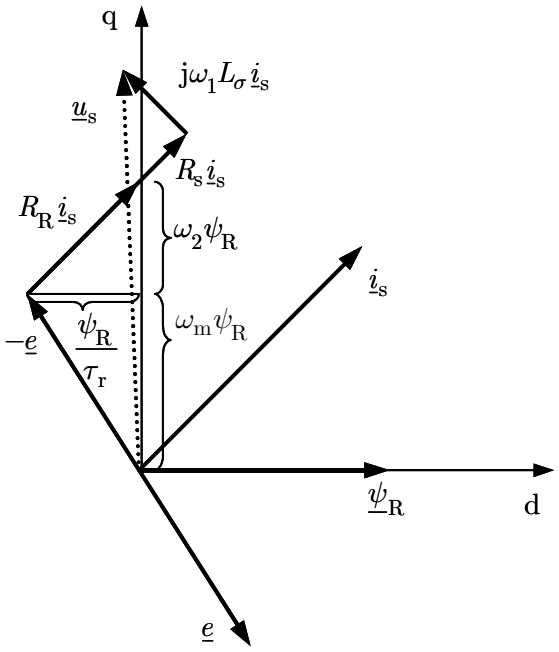

Fig. 2.4. Steady-state space vector diagram of an induction motor in the motoring mode when the stator frequency is non-zero.

However, at zero stator frequency, the induction motor rotor flux is unobservable from the stator current and voltage in steady state, even with exact knowledge of the motor parameters and an ideal motor. At zero frequency, (2.16) and (2.17) give $\underline{u}_\mathrm{s} = R_\mathrm{s}\underline{i}_\mathrm{s}$ and $\underline{e} = R_\mathrm{R}\underline{i}_\mathrm{s}$, but the speed ω_m and the rotor flux linkage ψ_R in (2.15) remain unsolvable. The space vector diagrams in Fig. 2.5 represent two different zero-frequency steady-state operating conditions for the same motor. In Fig. 2.5 (a), the rotor flux is higher and the speed is lower than in the diagram in Fig. 2.5 (b). Yet there is no difference in the stator voltage or current between the diagrams. The situation would be different if the speed ω_m were known. The angle of the stator current in the rotor flux reference frame would then be known as $\tan^{-1}(-\tau_\mathrm{r}\omega_\mathrm{m})$.

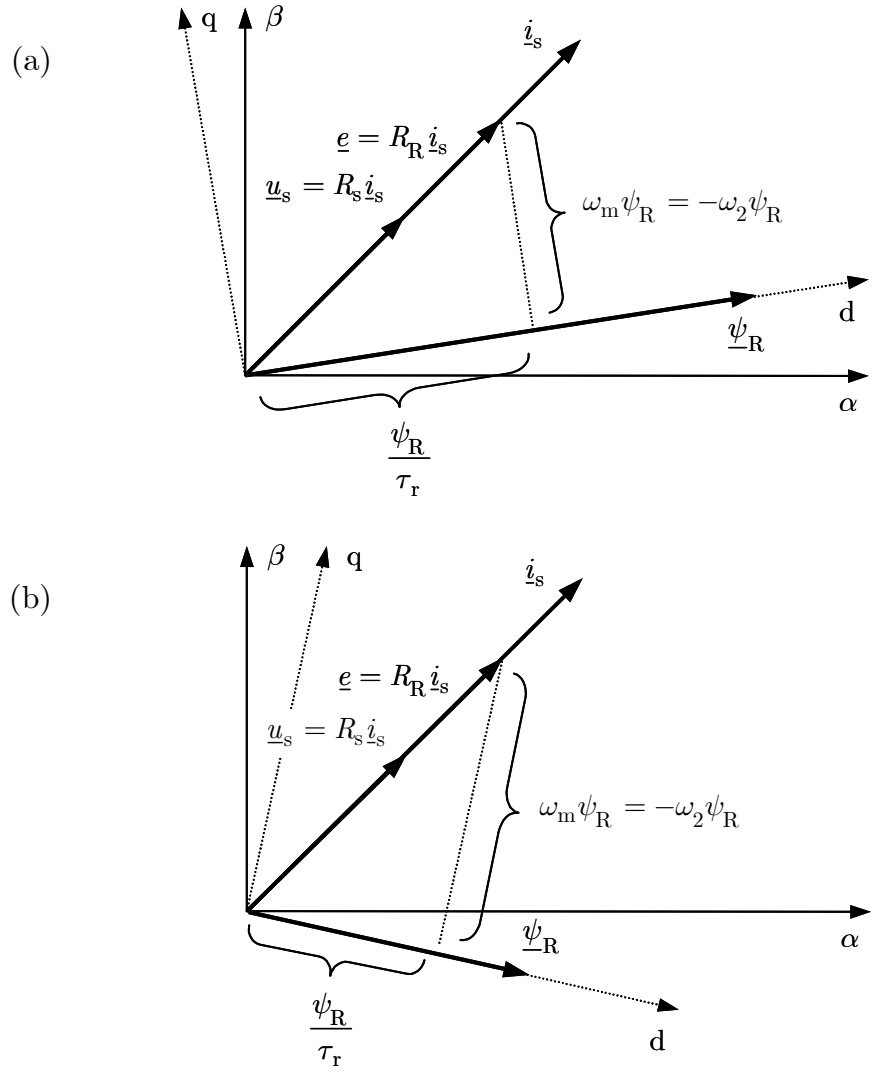

Fig. 2.5. Two different steady-state space vector diagrams of an induction motor under positive load torque at zero stator frequency. In (a), the rotor flux linkage is higher and the speed is lower than in (b), yet there is no difference in the stator quantities.

Hofmann and Sanders (1998) present a rigorous observability analysis starting from the state space representation of the electromechanical system, leading to the same conclusion: at zero fundamental frequency, the rotor dynamics are unobservable.

2.3 Principle of the method presented in this thesis

The angular speed of the rotor is governed by the equation of motion

$$\frac{\mathrm{d}}{\mathrm{d}t}\omega_\mathrm{m} = \frac{p}{J}(T_\mathrm{e} - T_\mathrm{L} - b\frac{\omega_\mathrm{m}}{p}), \tag{2.23}$$

where J is the total moment of inertia, b is the coefficient of viscous friction and T_L is the load torque. Combining (2.15) - (2.17), (2.22) and (2.23) leads to the signal flow diagram in Fig. 2.6, where it is assumed that the motor is current-fed. The close connection between the back-emf $\underline{e}$ and the stator voltage $\underline{u}_\mathrm{s}$, as shown in Fig. 2.3, is again evident.

The principle of the rotor flux orientation method presented in this thesis can be briefly introduced with reference to Fig. 2.6. An alternating current signal $i_\mathrm{cd}(t) = A\cos(\omega_\mathrm{c}t)$ is added to the quiescent flux-producing stator current component i_d0. The angular frequency ω_c of the signal is sufficiently large to produce no significant variation in the flux level. If there is a small orientation error $\varepsilon = \hat{\theta}_1 - \theta_1$ between the actual rotor flux angle θ_1 and the estimated angle $\hat{\theta}_1$, the actual stator current in the rotor flux reference frame will be approximately $\underline{i}_\mathrm{s} \approx i_\mathrm{d0} + i_\mathrm{cd}(t) + \mathrm{j}[i_\mathrm{q0} + \varepsilon i_\mathrm{cd}(t)]$, where i_q0 is the quiescent torque-producing stator current component. The variation of the term $\mathrm{j}\varepsilon i_\mathrm{cd}(t)$ is in phase with $i_\mathrm{cd}(t)$ if ε is positive, and in the opposite phase if ε is negative. Consequently, either an in-phase or an opposite-phase torque oscillation $T_\mathrm{ec}(t)$ will result. Provided that ω_c is low enough for the torque oscillation to affect the speed through (2.23), and omitting the

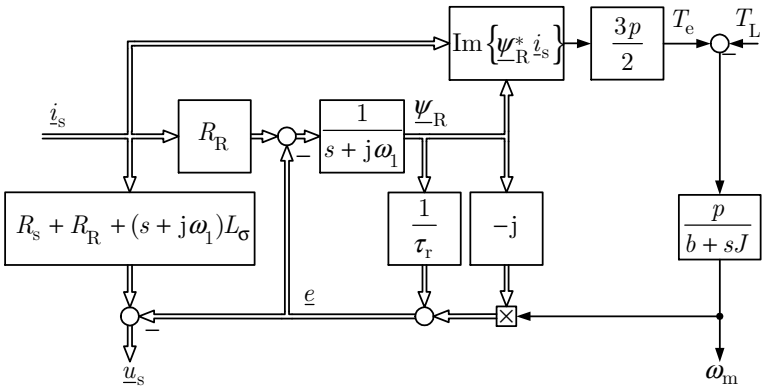

Fig. 2.6. Signal flow diagram of an induction motor in the reference frame attached to the rotor flux, corresponding to the dynamic Γ-equivalent circuit. It is assumed that the stator current is controlled by fast current control. Double lines indicate complex quantities (space vectors) whereas single lines indicate real quantities (scalars).

effect of the friction b, the resulting speed oscillation $\omega_{\mathrm{mc}}(t)$ will then be either lagging $i_{\mathrm{cd}}(t)$ by $\pi/2$ (corresponding to $\varepsilon > 0$), or leading $i_{\mathrm{cd}}(t)$ by $\pi/2$ (corresponding to $\varepsilon < 0$). Finally, the q component of the back-emf shows an oscillation $e_{\mathrm{cq}}(t) \approx -\omega_{\mathrm{mc}}(t)\psi_{\mathrm{R}}$. The phase of $e_{\mathrm{cq}}(t)$ depends on ε:

$$e_{\mathrm{cq}}(t) \sim \begin{cases} \cos(\omega_{\mathrm{c}} t + \pi/2), & \varepsilon > 0 \\ \cos(\omega_{\mathrm{c}} t - \pi/2), & \varepsilon < 0 \end{cases} \tag{2.24}$$

An error signal F_ε can be obtained by multiplying $e_{\mathrm{cq}}(t)$ by $\sin(\omega_{\mathrm{c}} t)$ and low-pass filtering. Thus the error signal has the property

$$\begin{cases} F_\varepsilon < 0, & \varepsilon > 0 \\ F_\varepsilon > 0, & \varepsilon < 0 \end{cases} \tag{2.25}$$

which can be used to drive ε towards zero.

3 Speed Sensorless Control of Induction Motors

The approaches to sensorless vector control of induction motors may be classified into four broad categories, as in Table 3.1. The categories are determined first by the motor model used, and then by the type of excitation given as input to the motor. In the table, the *fundamental-wave motor model* is basically that described in Chapter 2, whereas the *non-fundamental-wave motor model* is a model that deviates essentially from the assumptions listed in the beginning of Chapter 2. Introducing some constructional asymmetry into the rotor, for example, or taking the magnetic saturation into account, yields a non-fundamental-wave motor model. *Fundamental-wave excitation* means that in addition to the basic flux and torque-producing components, no extra voltage or current signal is intentionally fed into the stator winding. In steady state, the voltage (or current) fed into the motor is, in the ideal case, sinusoidal (or dc), without harmonics. *Signal injection* means that some time-varying voltage or current signal is intentionally added to the fundamental-wave excitation.

Obviously, the pure fundamental-wave approach, where the fundamental-wave motor model and fundamental-wave excitation are used, has less freedom in selecting the underlying principle for sensorless field orientation than the other approaches. However, it is the approach most generally applicable. Moreover, powerful tools and an understanding of the problem have accumulated over the years into a mature, yet still developing, state-of-the-art. In Section 3.1, the development and state of the fundamental-wave approach are briefly described.

TABLE 3.1. APPROACHES TO SENSORLESS CONTROL OF INDUCTION MOTORS.

	Fundamental-wave motor model	Non-fundamental-wave motor model
Fundamental-wave excitation	Section 3.1	Section 3.2
Signal injection	Section 3.3	Section 3.4

In principle, there are two possibilities with respect to combating the limitations of the pure fundamental-wave approach. First, it is possible to abandon the fundamental-wave motor model in favor of a more detailed one. Typically, the new motor model is *spatially anisotropic*, i.e., the impedance of the motor as seen from the stator terminals is not equal in different directions. Section 3.2 deals with this approach.

Second, it is possible to stay with the fundamental-wave motor model, but to enhance the fundamental-wave excitation in some way to either avoid the difficult operation at zero frequency in steady state, or to include a signal that gives rise to a useful response from the motor. This approach is discussed in Section 3.3.

In most signal-injection methods reported in the literature, both of the possibilities are used, i.e., the motor model is altered to include some physical feature omitted from the fundamental-wave model, while, at the same time, the excitation is enhanced to provide a signal exploiting that physical feature. Section 3.4 is devoted to these approaches.

3.1 Fundamental-wave motor model with fundamental-wave excitation

In the early days of frequency-converter-controlled induction motor drives, when the scalar control was mainly used, attempts to solve the low-speed problems of the speed sensorless control usually involved increasing the supply voltage when the operating frequency was close to zero. However, the exact amount of additional voltage is difficult to determine, and over-excitation of the motor usually occurred. Abbondanti (1977) describes the state-of-the-art, high-lighting the effect of the stator resistance estimate on the flux level, and gave one solution that worked well down to 1 Hz at 200 % load, both motoring and generating, using a 15 hp 60 Hz motor. The solution is based on the reactive power of the motor, and it has the benefit of being totally independent of the stator resistance. Yet, this approach falls in the category of scalar control methods.

Joetten and Maeder (1983) recognize the gap between the simple (sensorless) scalar control strategies with poor dynamics and the (sensored) high-performance vector control strategies. They proposed a sensorless slip frequency calculation scheme, based on the rotor back-emf estimation. The calculated slip frequency was fed to an inner slip frequency control loop, whereas the outer control loop could be for, for example, torque, speed or stator frequency regulation. The problems caused by the vanishing rotor back-emf at low speeds and an inaccurate stator resistance estimate were pointed out. The method worked well if the stator frequency was larger than ±3 % to ±5 % of the rated frequency. The dynamic response was improved

from that obtainable using a scalar control scheme, the speed settling time being about 100 ms.

The developments in the field of control theory during the 1950s and 1960s also influenced the way the control problems were handled in the field of motor drives. Starting from the state-space representation of linear time-invariant systems, new methods were adopted in the analysis and synthesis of control algorithms. Since the induction motor is a non-linear, time-variant system, either linearization through simplifying assumptions, or adoption of a control method for non-linear and time-variant systems, was needed. The Kalman filter is a celebrated stochastic system identification tool, introduced by R. E. Kalman in the 1960s (Åström and Wittenmark 1997). The filter gives an optimal identification result, provided the noise is white Gaussian. A variant of the filter called the Extended Kalman Filter (EKF) can be used for the identification of nonlinear systems. Hillenbrand (1983) proposes the use of the EKF in estimating the speed of an induction motor.

Another popular nonlinear control structure combines the system identification task with the control or regulator problem in an adaptive way. The Model Reference Adaptive System (MRAS) has originally been used for adaptive controller parameter adjustment by forcing the plant output to match an output obtained from a model of the desired performance (Åström and Wittenmark 1995). The MRAS structure can also be configured to use two different models for estimating the same quantity y. For the estimation, one of the models (the adaptive model) needs a set of unknown parameters, while the other model (the reference model) is independent of this set. The respective outputs of the two models, $\hat{y}_{\mathrm{a}}$ and $\hat{y}_{\mathrm{r}}$, are forced to agree by a controller adjusting the unknown parameter set. If the parameter set consists of only one parameter, and if the estimate $\hat{y}_{\mathrm{r}}$ provided by the reference model is correct, it is reasonable to believe that the parameter will get correctly identified. However, if there are more unknown parameters, there is a possibility of cancellation between the individual parameter errors.

Schauder (1992) adopts the MRAS in the speed estimation of an induction motor. The voltage model of (2.11) can be used to estimate the rotor flux linkage. Since the speed is not needed in (2.11), the voltage model was taken as the reference model. The current model of (2.7) can also be used for estimating the rotor flux linkage. Since (2.7) is dependent on the speed, the current model was adopted as the adaptive model. It is noteworthy that the rotor flux linkage and the speed are both identified by this MRAS structure. The application of (2.11) for the rotor flux linkage requires pure integration of the right-hand side of the equation. Schauder pointed out the practical problems of the pure integration and replaced the integrator with a low-pass filter. The current model had to be modified accordingly. Obviously, the quality of

the MRAS is dependent on the quality of the reference model. Peng and Fukao (1994) introduce an MRAS structure where the back-emf was used in the reference and adaptive models instead of the rotor flux, thus avoiding the problem of open-loop integration. Further, they proposed another MRAS structure where the cross product of the stator current and the back-emf is used, circumventing the problems associated with the stator resistance. The rotor time constant affects only the speed control accuracy, leaving the total leakage inductance and the magnetizing inductance the only motor parameters affecting the field orientation. Marwali and Keyhani (1997) have compared the rotor flux and back-emf-based MRAS speed estimators. They conclude that the low-speed performance of the back-emf-based one is better, but it is more difficult to design.

Bauer and Heining (1989) combine the voltage model and the current model in a position-sensored flux observer in such a way that, at low speeds, only the current model is used, while, at higher speeds, only the voltage model is used. The transition between the models is smooth and continuous. Jansen and Lorenz (1994) use a similar scheme, called Closed-Loop Flux Observer (CLFO). They also propose the observer structure to be used in sensorless flux estimation (Jansen and Lorenz 1993). There, the CLFO is used as the reference model, while the current model is still the adjustable model. The speed (and position) estimate is obtained from a mechanical system model incorporated within the adaptive controller of the MRAS. However, the authors state that "even this method is NOT a solution to fundamental zero speed limitations." Blasco-Gimenez et al. (1996a, 1996b) deal extensively with the performance limitations of the MRAS-based sensorless induction motor drives. The combined MRAS-CLFO of Jansen and Lorenz (1993), in particular, is analyzed, since the authors consider this structure the best MRAS flux and speed estimator available. "It is concluded that speed and load torque rejection bandwidths comparable to sensored vector controllers cannot be obtained without online parameter tuning."

The observer theory (Luenberger 1971) is another achievement of control theory of the 1960s that has penetrated the motor drive field. It provides a tool for reconstructing missing state-variable information necessary for control. The inputs and outputs (i.e., available states) of the system are the inputs of the observer, whose output is an approximation of the *full-order* state vector of the system. A *reduced-order* observer is also possible, where the states already available are not reconstructed. For example, if the stator current and rotor flux linkage of an induction motor are taken as state variables, a reduced-order flux observer constructs only an estimate of the missing state, i.e., the rotor flux linkage. The inputs to the observer are the stator voltage and the stator current. The speed enters the observer

via the system matrix. Verghese and Sanders (1988) lay the ground for the use of observers for flux estimation in induction machines. They also point out that the Kalman filter is just a special case of the observer with observer gain yielding the minimum least-square estimation error when the noise is white Gaussian. At the time of their writing, the flux estimation problem was mainly addressed in a sensored setting. The authors saw, however, that there is a "clear trend toward replacing sensors that are expensive, unreliable, or hard to install, with less costly measurement schemes [...]"

Tajima and Hori (1993) use the MRAS structure of Schauder (1992) only for speed estimation, while a speed-adaptive reduced-order flux observer is also used for the flux linkage estimate. In this observer, the estimated speed is also used in the observer gain matrix to make the observer pole-placement a function of the speed.

Harnefors (1998) compares the full-order flux and speed observer with an EKF and concludes that the full-order observer is more robust to parameter errors, while the EKF provides a flux estimate with less noise. Harnefors (2000) studies the instability phenomena of sensorless indirect field orientation (IFO) that are not present in the sensored operation, and proposes remedies, which, however, are derived on the assumption of constant-speed and constant-torque. He also finds out that the full-order observer for speed estimation is superfluous; the same asymptotic speed estimate can be obtained directly by solving it from the q component of the stator voltage in (2.16).

Harnefors (2001) continues by analyzing reduced-order observers in rotor-flux-oriented vector control. He points out that, by selecting the observer gain properly, either the voltage model or the current model is obtained. Hence, making the observer gain speed dependent via a gain-scheduling scheme, seamless transition from the current model to the voltage model is obtained, as in the CLFO of Jansen and Lorenz (1994). Several other strategies for the observer gain are also analyzed; one of them yields an observer independent of the stator resistance since the stator frequency is calculated using the instantaneous reactive power, resembling the MRAS approach of Peng and Fukao (1994).

Regardless of the type of fundamental-wave observer used, and even with accurate model parameters, there is, in addition to the unobservability problem at zero frequency, an unstable region encountered at low speeds in the regenerating mode. Paying attention to this region, Kim et al. (2003) introduce a stator flux oriented, voltage-model-based sensorless vector control scheme, where the stator flux is first estimated using the voltage model, and an estimate of the d component of the stator current is calculated from the flux estimate. A current error term is obtained as the difference between the measured d component and this estimate. The sign of

the current error, as well as the sign of the flux angle and magnitude errors, are shown to depend on the sign of the error in the stator resistance estimate, the sign of the flux rotation, and the sign of the torque-producing current. The dependency is used to correct the flux estimate in a simple manner, called the Quadrant Error Compensation Rule (QECR). Experimental results, obtained in the presence of a considerable error in the stator resistance estimate, indicate stable operation under full-load torque, even at zero frequency and in the regenerating mode. Hinkkanen and Luomi (2003) introduce a scheme remotely resembling the QECR for stabilizing the full-order speed-adaptive observer in the low-speed regenerating mode. They analyze the conventional speed-adaptation law in the steady state for a given speed estimation error. They find that the unstable region can be avoided if, in addition to the current estimation error perpendicular to the estimated rotor flux, the error parallel to the estimated rotor flux is also used in the adaptation law. In practice, they rotate the current estimation error at low speeds in the regenerating mode. Experimental results demonstrate the effectiveness of the method. However, an accurate stator resistance estimate is still needed for stable operation in the regenerating mode.

A vast number of variants and combinations of the principles discussed above have been proposed for the sensorless vector control of induction motors. In addition, soft computing methods (neural networks, fuzzy control, genetic algorithms) not treated here have gained popularity in motor control applications. However, the limitation of the fundamental-wave motor model at zero frequency, combined with the unavoidable uncertainty in the parameter estimates and the measurements, reduces the usefulness of all these methods when the frequency is close to zero in steady state.

3.2 Non-fundamental-wave motor model without signal injection

In those sensorless control schemes where no additional excitation (signal injection) is provided from the stator supply side, the magnetic saturation of the air-gap flux and the effects of rotor slotting are the most commonly used non-ideal features of the induction motor. The saturated air-gap flux induces a third-harmonic stator phase voltage (Moreira and Lipo 1992), which can be detected from the zero-sequence voltage, provided the neutral of a wye-connected motor is available for measurement of the phase voltages. Based on the third-harmonic voltage, the location of the air-gap flux, and thus also the flux- and torque-producing components of the stator current, can be determined (Moreira et al. 1991, Bonanno et al. 1997). At zero stator frequency, however, no voltage is induced since the air-gap flux and its space harmonics are stationary relative to the stator. Another problem of air-gap-

saturation-based methods is that the level of saturation has to be considerable in order to have sufficient gain for the error signals.

There are also higher-order harmonics in the air-gap field that are caused by the rotor slots (Ishida and Iwata 1982). Consequently, the zero-sequence stator voltage induced by the air-gap field contains the corresponding rotor slot harmonics. The frequencies of these harmonics are proportional to the rotor speed. Jiang and Holtz (1997) tune the center frequency of an adaptive band-pass filter to track the dominant rotor slot harmonic. The speed signal is subsequently used for parameter adaptation in a stator-field oriented controller. However, the amplitude and frequency of the slot harmonic voltage approach zero as the speed approaches zero. Measuring the zero-sequence stator voltage also requires a wye-connected stator winding.

Rotor slot harmonics can also be detected from the stator current spectrum. Hurst et al. (1995) take the CLFO of Jansen and Lorenz (1993) and augment it with a harmonic-based speed detector. The speed detection is reliable only if the motor operates in the steady state for a sufficiently long time for the spectrum estimation process. The estimated rotor speed signal is used to tune the uncertain parameter estimates for the moment of inertia $\hat{J}$, the viscous friction $\hat{b}$ and the rotor time constant $\hat{\tau}_\mathrm{r}$ of the CLFO, which then provides the continuous speed estimate.

In spectrum estimation, there is a trade-off between accuracy and speed. To probe this trade-off, FFT-based and non-parametric spectrum estimation techniques for extracting the rotor speed information from the stator current are compared by Hurst and Habetler (1997). They conclude that non-parametric methods are faster, while FFT-based methods yield more accurate steady-state results. However, a fundamental problem in spectrum estimation cannot be avoided: since the sampling is usually carried out over a fixed number of cycles, the sampling time needed increases when the frequency decreases. As the stator frequency gets below 1 Hz, the slot harmonic spectrum becomes increasingly noisy. In addition, at low frequencies, the spectral separation of all the different signals that tend to zero at zero speed or zero stator frequency becomes difficult. However, it should be kept in mind that the estimation of the rotor position is a more challenging task than the estimation of the flux linkage.

3.3 Fundamental-wave motor model with signal injection

Respecting the limitation of the fundamental-wave model that steady-state zero-frequency operation is not possible, schemes have been proposed where continuous zero-frequency operation is avoided. Depenbrock et al. (1999) propose a variation to the slip frequency through stator flux amplitude control such that stationary operation in a gap around zero stator frequency is avoided. Kubota et al. (2002)

propose a similar method for controlling the rotor flux level to avoid zero-frequency operation. Both of these methods can be called signal-injection methods in the sense that the field-weakening signal for the flux reference is superimposed on the flux reference.

Circumventing the problem of zero stator frequency operation is possible by fluctuating the rotor flux reference continuously at a very low frequency (Takeshita et al. 2002). The idea is to detect the speed-emf (the term $\mathrm{j}\omega_\mathrm{m}\psi_\mathrm{R}$ in the back-emf) even at zero stator frequency because the fluctuation makes the rotor dynamics observable, so that the stator flux linkage derivative $\underline{u}_\mathrm{s} - R_\mathrm{s}\underline{i}_\mathrm{s}$ is not zero, but its locus is an ellipse around the origin. For a four-pole, 2.2 kW, 200 V, 60 Hz motor a 2 Hz fluctuating signal with an amplitude of 10 % of the nominal flux-producing current is added. Even if zero-frequency operation under 150 % load torque is achieved, the speed reportedly has to be above 40 rpm (0.022 p.u.) for successful detection of the speed-emf.

Estimating the rotor speed based on extra rotor synchronous current control (Kaku et al. 1998) is based on adding a test signal voltage of adjustable frequency on the stator voltage. If the injected voltage rotates synchronously with the rotor, no rotor current will be induced. Identifying the extra rotor current, and controlling its amplitude to zero by adjusting the frequency of the voltage signal, is the basis of speed estimation in this method. However, the calculation of the rotor current is based on knowledge of the stator flux, so low-speed problems may be expected.

Detection of the response of the angle of the back-emf, i.e., the response in $\arg(\underline{e}^\mathrm{s})$, to a low-frequency alternating test signal current added in the flux-producing component of the stator current was proposed by Sng et al. (1998). A four-pole, 2 hp, 200 V, 60 Hz motor was used and a 20 Hz, 0.32 A test signal was added to the flux-producing current of 2.5 A. The method is based on an assumption that all the variation in $\arg(\underline{e}^\mathrm{s})$ correlating with the test signal is due to the test-signal-induced variation in the rotor flux angle $\arg(\underline{\psi}_\mathrm{R}^\mathrm{s}) = \theta_1$. According to (2.8), this assumption means that the speed ω_m is essentially constant. Adjusting the test signal in the direction of the rotor flux drives the angle variation to zero.

The work reported in this thesis (Publications [P2] – [P9]) also falls into the category of methods using the fundamental-wave motor model with signal injection. A low-frequency ac current test signal is superimposed on the flux-producing stator current component. The test signal creates an oscillation in the electromagnetic torque if its direction is not aligned with the rotor flux. Assuming a moment of inertia low enough for the speed to react to the torque oscillation, there will be a discernible response in the q component of the back-emf, which can be extracted from

the stator voltage. Adjusting the test signal in the direction of the rotor flux drives the back-emf response to zero.

Since the test signal employed in this thesis is practically identical to the one used by Sng et al. (1998), it is interesting to compare the methods. The method of Sng et al. is based on the rotor flux dynamics, leading to the response in the angle of the back-emf in the stationary reference frame, while the method presented in this thesis is based on the mechanical dynamics, leading to the q component response in the back-emf in the rotor flux reference frame. At zero speed, the response in the q component of the back-emf can be interpreted as a response in the angle of the back-emf, and vice versa. It should also be noted that, since both methods use an alternating test signal in the estimated direction of the flux, they share the benefit that torque ripple, audible noise and vibration are reduced when the orientation error is zero.

3.4 Non-fundamental-wave motor model with signal injection

High-frequency signal injection

Most of the signal-injection methods reported in the literature superimpose a high-frequency signal (ca. 250 - 500 Hz) of relatively small amplitude on the stator voltage, and the response of the motor to the signal is extracted from the corresponding high-frequency stator current (Jansen and Lorenz 1996, Ha and Sul 1999, Ha et al. 2000, Degner and Lorenz 2000, Teske et al. 2001b, Cilia et al. 1997). The high-frequency signal is easier to apply as a voltage than a current (Ribeiro et al. 1998) because a high-bandwidth current controller is not needed. On the other hand, the current controller bandwidth must be limited so that the current controller does not interfere with the voltage signal and its response in the current.

The superimposed voltage or current can be either a balanced three-phase (rotating) signal, or an alternating one. In the latter case, the alternation is given in a certain direction in the reference frame of the controller. Most often, the alternating signal is applied in the estimated direction of the flux. Scanning the air-gap periphery by an alternating signal, the direction of which is slowly rotated, has also been proposed (Drevensek et al. 2002). The response to the alternating signal is evaluated in fixed directions relative to the signal direction (e.g., the signal direction itself, or the direction perpendicular to it, or in two mutually orthogonal directions symmetric about the signal direction).

The response of the stator current of an induction motor to a high-frequency voltage (or vice versa) is dominated by the leakage inductance. The motor models

used in conjunction with the high-frequency signal injection usually assume a spatial variation of the leakage inductance along the air-gap periphery. The spatial variation can be caused by local saturation, while, in an ideal case, the most saturated region, as found by the signal-injection method, is the region where the air-gap flux is the strongest. The variation of the leakage inductance can also be linked directly to the rotor position through the permeance variation caused by the rotor slots. To create a stronger position-dependent variation, it is even possible to modulate the rotor leakage inductance through varying the widths of the rotor slot openings over one pole pitch (Jansen and Lorenz 1995). In the literature, this kind of saliency is called an *engineered saliency*. Cilia et al. (1997) engineer a rotor resistance variation over one pole pitch in a double-cage rotor. Staines et al. (1999) propose modulating the rotor resistance in the same way, but, instead of a continuous signal injection, they use periodic high-frequency bursts to determine the incremental rotor position. The application of high-frequency signal injection to detect the air-gap permeance variation caused by the stator and rotor slots has also been proposed (Degner and Lorenz 2000, Teske et al. 2001b).

A special class of signal-injection methods relies on the inherent transient excitation provided by the pulse-width-modulated output voltage waveform of the inverter supplying the motor. As one of the inverter output phase potentials is switched from the negative dc-bus potential to the positive one, or vice versa, there will be a step change in the stator voltage space vector. According to (2.1), the voltage step will take place in the spatial direction of the switching phase. The stator current will show a transient step response. Analyzing the transient response in time domain immediately after the voltage step will give information about the transient impedance of the motor. Schroedl (1992) does pioneering work in this area with the introduction of the method of INdirect Flux detection by On-line Reactance Measurement (INFORM). Holtz et al. (1997) use the PWM switching to determine the instantaneous rotor position through the leakage inductance variation caused by the rotor slotting. The method assumes a wye-connected stator winding. A dual of the method of Holtz (1997), applicable for delta-connected motors, is proposed by Caruana et al. (2003). They measure the derivative of the zero-sequence current, and use the information for rotor flux tracking.

Problems of high-frequency signal injection

Injecting the high-frequency signal and extracting and analyzing the response are not a key problem in the high-frequency signal-injection methods. Instead, there are underlying problems associated with the basic phenomenon of leakage inductance variation. Since both the saturation-induced and rotor-position-dependent variations

of the leakage inductance are always present in the overall variation, some means for their separation must be provided. Especially, if the position-dependent variation is to be tracked, the saturation-induced variation must be carefully compensated (Briz et al. 2001a, Briz et al. 2002, Teske et al. 2000). The saturation-induced saliencies are usually larger in amplitude than the position-dependent ones, unless an engineered saliency strong enough is introduced. Teske et al. (2001a) also point out that, since the high-frequency voltage injection is usually performed open-loop, any voltage distortion caused by the non-ideal inverter (mainly due to the dead-time effects) may have detrimental effects on the position tracking. A compensation strategy Space Modulation Profiling (SMP) to compensate for both the saturation- and inverter-induced saliencies is presented (Teske et al. 2001a). Harmonics caused by transients in the fundamental current close to the frequency of the injected signal may also interfere with the tracking of the saliency. A fundamental-current observer to compensate the interference and thus increase the dynamic performance of the signal-injection method has been proposed (Briz et al. 2000, Briz et al. 2001b).

An even more fundamental problem lies in the fact that the saturation of the air-gap flux path and the saturation of the leakage paths are usually not in the same region on the air-gap periphery (Aime et al. 1998, Drevensek et al. 2002). The individual motor design affects the saturation behavior most notably through the rotor slot geometry (Wolbank and Haidvogl 2000, Wolbank et al. 2002a). The slot openings play an especially crucial role in being open, semi-closed or closed, thus affecting the saturation characteristics of the rotor leakage path, as already mentioned by Jansen and Lorenz (1996). The rotor lamination has also been reported (Wolbank et al. 2002b) to have an effect on the leakage inductance variation.

Interacting with the design-specific dependencies, the operating point of the machine has an influence on the final pattern of the leakage inductance variation. Load, as pointed out already by Schroedl (1992), and flux level are the major contributors to the local saturation. Aime et al. (1998) have carried out extensive tests to detect where a machine saturates under different operating conditions. They conclude: "[...] saturation-induced saliencies can be significant at all flux levels and are not fixed in position relative to any component of flux." Rather, the saliency is determined by the combined effect of the magnetizing and leakage fluxes, representing a problem for saliency-based flux angle estimation methods. The frequency of the injected signal determines how deep into the rotor its influence can penetrate, thus defining the region in space that is actually evaluated by the signal-injection method. In the measurements, they used the carrier frequency signal-injection method proposed by Jansen and Lorenz (1996) for detecting the location of the saliency. Thus the conclusion is especially valid in respect to that method.

Signal injection and air-gap flux saturation

In addition to the methods based on the third-harmonic phase voltage explained in Section 3.2, the saturation of the air-gap flux can be also exploited in high-frequency voltage signal injection as proposed by Consoli et al. (2000a). Adding a rotating high-frequency voltage on the fundamental stator voltage creates a small-amplitude high-frequency rotating field that is superimposed on the main field. The high-frequency field modulates the saturation level of the magnetizing inductance, giving rise to an additional zero-sequence component of the air-gap flux, which in turn induces a corresponding zero-sequence stator voltage component. The frequency of the rotating high-frequency field is the difference between the frequency of the injected voltage and that of the main field. Consequently, the high-frequency zero-sequence air-gap flux will persist even at zero fundamental frequency. Consoli et al. (2000b) propose a variant of the scheme where the high-frequency voltage is alternating instead of rotating. Tracking the maximum of the generated zero-sequence voltage component ensures that the alternation is aligned with the air-gap flux. Thus the method is free from the ambiguities associated with the saturation of the leakage inductance. However, like other methods using the zero-sequence voltage, this method is dependent on the measurement of the phase voltages. The authors state that the measurement does not necessarily need access to the neutral point of the machine. It is also pointed out that, in contrast to most of the other high-frequency voltage injection methods, the response is extracted from a voltage signal instead of (a weak) current signal.

Due to saturation, the current transfer from stator into rotor takes place with less gain in the direction parallel with the rotor flux than in the direction perpendicular to it. This phenomenon can be used to detect the rotor flux angle (Blaschke et al. 1996). A low-frequency alternating test current is added to the flux-producing stator current component, and the resistive voltage drop in the rotor, caused by the test-signal-induced rotor current, is extracted from the stator voltage. Adjusting the direction of the test signal so that the direction of the rotor voltage drop is aligned with the test signal leads to rotor flux orientation. The method is only used at low frequencies to correct a fundamental-wave observer. Experimental results for a 25 kW motor using a 20 Hz test signal of 0.25 p.u. are shown. However, zero frequency operation is shown only at 75 % load torque.

3.5 Summary of sensorless control methods

The sensorless control methods discussed in this chapter, and already outlined in principle in Table 3.1, are mapped in Table 3.2 according to (a) the underlying

TABLE 3.2. SUMMARY OF SENSORLESS CONTROL METHODS.

(a) / (b)	Fund.-wave motor model	Fund.-wave motor model and avoiding zero-frequency operation	Fund.-wave motor model and mechanical reaction	Saturation of leakage flux	Saturation of air-gap flux	Slot harmonics	Engineered leakage inductance variation	Engineered rotor resistance variation
No additional signal	Fund.-wave observers (Sec. 3.1)				Moreira Bonanno (Sec. 3.2)	Jiang Hurst (Sec. 3.2)		
PWM switching				Schroedl (Sec. 3.4)	Caruana (Sec. 3.4)	Holtz (Sec. 3.4)		
Rotating high-frequency voltage				Jansen (Sec. 3.4)	Consoli (Sec. 3.4)	Teske Degner (Sec. 3.4)	Jansen (Sec. 3.4)	Cilia (Sec. 3.4)
Alternating high-frequency voltage				Ha (Sec. 3.4)	Consoli (Sec. 3.4)			
Low-frequency flux level fluctuation		Depenbrock Kubota Takeshita (Sec. 3.3)						
Alternating low-frequency current	Sng (Sec 3.3)		Leppänen (Sec. 3.3)		Blaschke (Sec. 3.4)			
Scanning high-frequency voltage				Drevensek (Sec. 3.4)				
High-frequency voltage burst								Staines (Sec. 3.4)
Adjustable frequency voltage	Kaku (Sec. 3.3)							

physical feature or phenomenon that the method is based on, and (b) the character of the test signal. The purpose of the table is not to be a complete picture of the state-of-the-art, but rather to provide a common framework for the various methods in a simple manner, thus positioning the method presented in this thesis into its context.

Often, control methods based on the non-fundamental-wave motor model or signal injection are combined into a fundamental-wave method in order to enhance the performance of the latter in the difficult low-speed operation range. In Publications [P3] – [P7] and [P9] the correction term obtained from the signal-injection method was added to the feedforward-loop of a very primitive implementation of the voltage model. The combination can also be done via parameter adaptation (e.g., Jiang and Holtz 1997, Hurst et al. 1995) or by introducing a correction term into the feedback-loop of the fundamental-wave observer as was done, for example, by Ide et al. (2002) and in Publication [P8].

4 Description of the Laboratory Setup

The experimental results presented in Publications [P2] – [P8] were all obtained in a laboratory setup equipped with a standard 2.2 kW, 400 V, 50 Hz, four-pole induction motor. In this chapter, the setup is described in more detail.

4.1 Hardware

An overview of the system is shown in Fig. 4.1 and data relating to the hardware are given in Table 4.1. The induction motor (IM) is loaded by a permanent magnet synchronous motor (PMSM). Both motors are driven by frequency converters (VLT 5004 and Bivector) equipped with brake resistors (BR). The system is controlled by software running on a DS1103 PPC processor board in a PC. The system is dedicated to experimental studies of induction motor control. The synchronous motor drive is a standard servo drive, and used only for creating suitable load torque (or speed) profiles. The hardware of the induction motor drive allows flexible implementation of different control algorithms.

The hardware interface between the VLT 5004 frequency converter and the DS1103 processor board was originally developed at the Aalborg University (Teodorescu et al. 2000). The VLT 5004 frequency converter was modified from an industrial standard product to provide an interface directly at the power circuit level: PWM gate signals provide the input to the drive, while the measurements of the dc-link voltage and the phase currents are used for feedback. The Bivector load drive is controlled by an analogue torque reference, which can also be given manually. The actual speed and shaft torque are measured using an encoder (ENC) and torque transducer (TT). A photograph of the setup is in Fig. 4.2.

In the experiments presented in this thesis, the switching frequency of the inverter was 5000 Hz, and a sampling period of 200 μs was used in the measurements. Due to signal noise, the measured dc-link voltage was digitally low-pass filtered at a bandwidth of 80 Hz. The dc-link voltage was input to the modulator in the software together with the stator voltage reference. A fixed dead time of 2 μs was inserted between the turn-off of one IGBT and turn-on of the other

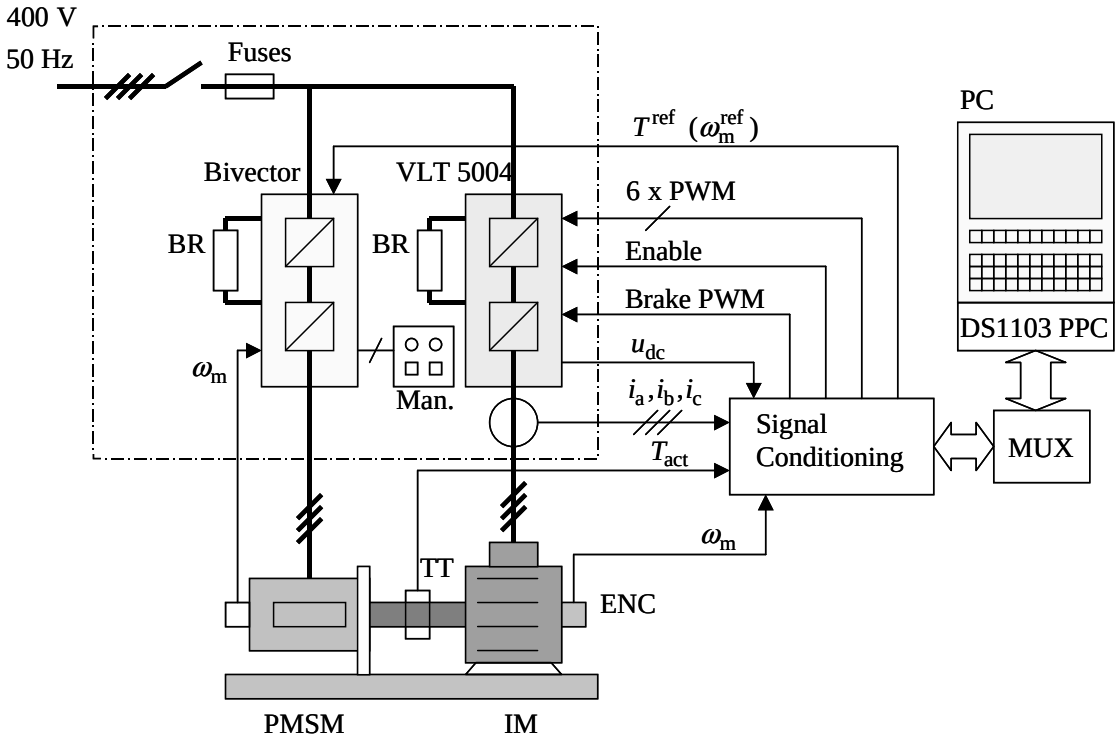

Fig. 4.1. The laboratory setup. The IM drive is loaded by a permanent magnet servo-drive. The control software runs on the DS1103 PPC board in the PC. The PWM gate signals are the input to the IM drive. The dc-link voltage and the phase currents are used for feedback. The load drive is controlled by an analogue reference, which can also be given manually. The speed and shaft torque are monitored using an encoder (ENC) and torque transducer (TT).

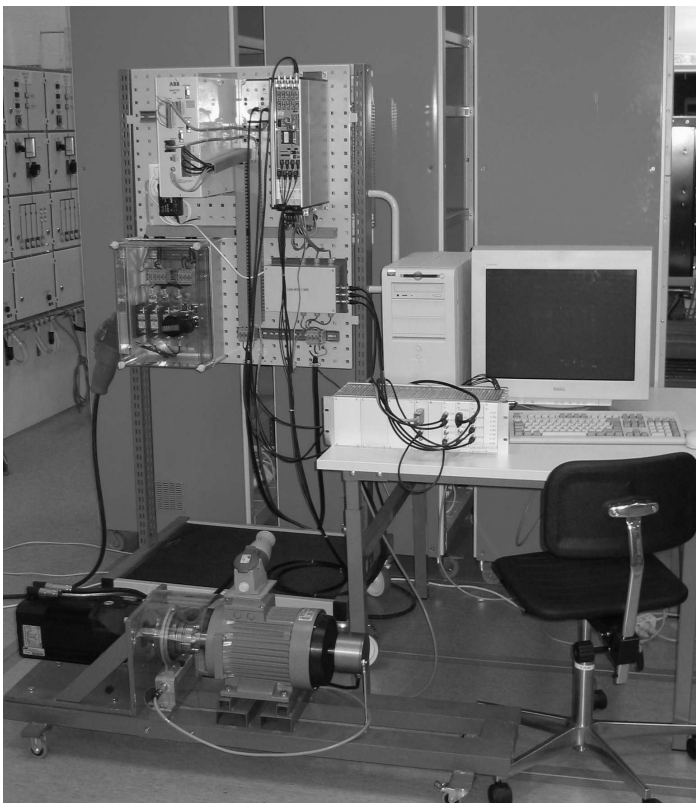

Fig. 4.2. Photograph of the setup. The layout follows that of Fig. 4.1, except for the location of the disconnect switch and fuses.

TABLE 4.1. DATA OF THE LABORATORY HARDWARE.

Item	Manufacturer and Type	Data
Induction motor (IM)	ABB M2AA 100LA 3GAA102001-ADA	380 – 420 V, 50 Hz, 1430 rpm, 2.2 kW, 5 A, $\cos\varphi = 0.81$, $J = 0.0069$ kgm^2
Frequency converter for the IM	Danfoss VLT5004 (modified for lab. use)	In: 380 – 500 V, 50/60 Hz Out: 0 – U_{in}, 0 – 1000 Hz, 5.6 A
Processor board	dSPACE GmbH DS1103 PPC	PowerPC 604e, 400 MHz, 2MB SRAM, 128 MB data logging memory, Slave DSP F240
Servo motor (PMSM)	ABB 8C523000YA02SL3MB	315 V, 3000 rpm Cont. stall torque 21.5 Nm, 14.1 A, $J = 0.0040$ kgm^2
Frequency converter for the PMSM	ABB Bivector535 “25”	In: 400 V, 26.5 A Out: 400 V, 25 A, 17.3 kVA
Current transducers (CT)	LEM LA 55-P/SP1	0 – 200 kHz (-1 dB) 25 A : 50 mA, ±0.9 %
Incremental encoder (ENC)	Leine&Linde AB 18690311	2048 ppr
Torque transducer (TT) and coupling	Hottinger Baldwin Messtechnik GmbH K-T10F-050Q-SU2-G-1-W1-Y and BSD Modulflex	50 Nm, 15000 rpm, 0 … 1 kHz (-3 dB), ±0.2 %, $J = 0.0031$ kgm^2, torsional stiffness 24 kN/rad

IGBT in the same inverter phase, and the compensation of the dead time (when implemented) was added to the duty cycles of the inverter phases just prior to feeding them into the modulator. This way, the stator voltage reference could be taken as the estimate of the actual stator voltage. All three phase currents were measured for current control.

4.2 Software

An illustration of the software environment in the setup is given in Fig. 4.3. The development software comes from two sources. First, for creating the controller algorithm, the MATLAB/Simulink software of MathWorks Inc. is used. The controller is interfaced to the real system via graphical I/O-interface blocks provided by dSPACE GmbH for their DS1103 PPC hardware. The Simulink Real-Time Workshop software generates executable C-code from the graphical representation of the model. Then, the Real-Time-Interface software of dSPACE GmbH generates downloadable code from the C-code, and starts the real-time processor.

The process can be commanded and monitored via the ControlDesk software of dSPACE GmbH. Additionally, the MLIB/MTRACE libraries of dSPACE GmbH make it easy to record signals into the workspace of MATLAB for post-processing and documentation.

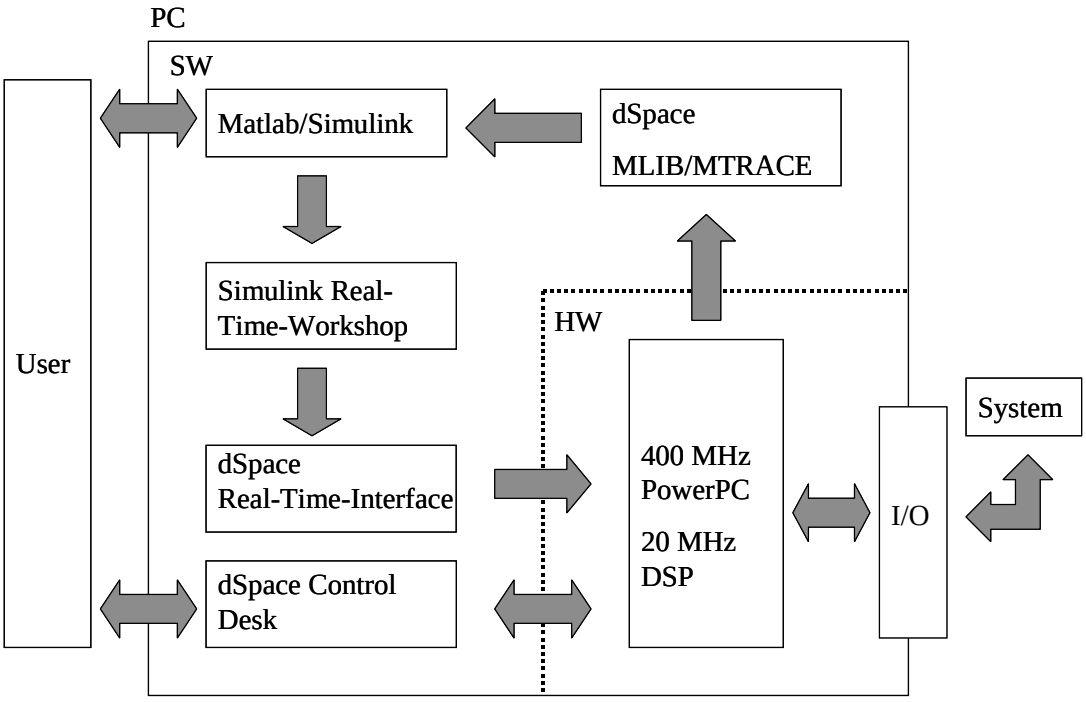

Fig. 4.3. Overview of the computing environment in the laboratory setup.

In the experiments reported in this thesis, the whole control algorithm was run at a sampling time of 200 μs. The actual turn-around time of the algorithm was in the range of 60 μs to 80 μs, mainly depending on the dimension of the moving average filters (i.e., the test signal period T_c).

More information about the hardware and software described in this chapter is available at the following internet-addresses: www.abb.com, www.danfoss.com, www.dspace.de, www.hbm.de, www.leinelinde.se, and www.mathworks.com.

5 Summaries of the Publications

Publication [P1]

The back-emf, as defined in Publication [P1], can be considered to be a useful halfway stop on the way from the stator quantities to the rotor flux linkage. The space vector of the back-emf is directly proportional to the rotor flux linkage vector, even though their ratio is complex, and depends on the speed of the rotor. The publication describes a method for evaluating the back-emf from the measured stator current and the known stator voltage, without prior knowledge of any motor parameters. The method is based on precise timing of the current measurement within a PWM cycle and solving the stator voltage equation with the knowledge of the change of the time derivative of the current. Simulation results in the publication support the validity of the method.

In practice, however, the method is of little use: the sampling rate and computational burden associated with the measurements is considerable, while measurement noise has detrimental effects on the differentiation of the stator current. Moreover, the magnetic saturation and the skin effect introduce a fast time variation of the transient time constant. Consideration of these parasitic, non-ideal phenomena in the motor led the author into the study of flux observers based on the saliencies caused by the parasitic effects.

Publication [P2]

Publication [P2] originated from a casual laboratory experiment. An unloaded motor was magnetized using a dc voltage, upon which a 10 Hz alternating component was superimposed. The spatial direction of the superimposed ac voltage was rotated slowly by 360 electrical degrees in order to see whether the corresponding alternating current component depends on the direction of the ac voltage. Indeed, a dependency was found, but it could not be attributed to any parasitic saliency effect in the electro-magnetic model of the motor. Instead, the reaction of the mechanical system

to the ac signal was found to give rise to a 10 Hz component in the back-emf. The amplitude and phase angle of this component appeared to be strongly influenced by the direction of the ac voltage relative to that of the dc voltage (i.e., the direction of the rotor flux).

Publication [P2] explains and analyzes the phenomenon in terms of low-frequency impedances of the electromechanical system. Based on the analysis, the relevance of the total moment of inertia in the system is pointed out. It is also suggested that the phenomenon could be used for a scheme to track the rotor flux angle.

Publication [P3]

The first implementation of the tracking controller for the rotor flux angle was proposed in Publication [P3]. In the implementation, there is a simple voltage-model-based fundamental-wave model providing a crude estimate of the rotor flux angular frequency. The tracking controller is used to correct that estimate. Instead of a voltage signal, an ac current test signal is employed. The signal is superimposed on the magnetizing component of the stator current. The extraction of the relevant back-emf-component from the stator voltage and stator current is described, together with a demodulation scheme for creating an error signal that is proportional to the error angle of the field orientation. The error signal is forced to zero by a Proportional-Integral controller, which adjusts the estimate of the rotor flux angular frequency. The estimate of the rotor flux angle is obtained by integrating the angular frequency estimate.

The proposed scheme is supported by simulation results: the steady-state error in the estimated rotor flux angle approaches zero. The controller shows stable operation both at zero speed and zero frequency under full torque. The dynamic performance is only moderate. Errors in the motor parameters are shown to have some effect on the behavior of the controller. The motor model, the current measurement and the PWM-inverter are assumed to be ideal in the simulation.

Publication [P4]

The system of Publication [P3] was implemented in a laboratory setup, and experimental results of the tracking controller were first reported in Publication [P4]. The phasor notation and phasor diagrams are used to explain the underlying phenomenon in the electromechanical system. The simulated controller signals from the stator voltage and back-emf to the error signal are shown, together with the actual error angle, illustrating the operation principle of the controller. A comparison of simulated and real test sequences gives insight into the operation of the controller.

Sustained zero-frequency operation under full torque is demonstrated. The experimental controller is shown to tolerate load torque steps of 50 % of the rated torque at zero speed. Experiments also indicate that the controller tolerates a variation of about 20 % in the estimates of the motor parameters.

Publication [P5]

Publication [P5] is mainly a presentation of further experimental results, obtained from practically the same setup that was used in Publication [P4]. Fast and slow speed reversals under rated torque, together with load torque steps of about 50 % of the rated torque, are shown. To demonstrate the capability of the controller to operate in all four quadrants close to zero frequency, a special sequence is carried out. In the sequence, the speed reference is varied sinusoidally with a period of 20 seconds and amplitude of 48 rpm, while the load torque is simultaneously varied with a period of 400 seconds and amplitude of 15 Nm.

Publication [P6]

The effect of parameter errors on the tracking controller is analyzed in Publication [P6]. In this publication, a distinction is made between the observer and controller parts of the tracking controller. It is the observer part that is more relevant in this thesis. The steady-state analysis suggests that the parameter errors have almost no effect on the remaining error angle when the error signal is controlled to zero. The conclusion is supported by experimental results from extremely slow speed reversals under rated load torque, obtained after purposefully detuning the controller.

The results of Publication [P6] encouraged the author to simplify the controller structure considerably from that used in Publications [P3] – [P5]. In particular, the terms including the stator resistance and total leakage inductance in the voltage model and in the extraction of the back-emf response could be removed altogether.

Publication [P7]

Publication [P7] was mainly motivated by comments from the reviewers and readers of Publications [P2] – [P5]. In the publication, the result of a more detailed derivation of the steady-state error signal is given. Due to limited space, the derivation of the back-emf response to the current signals was omitted from Publication [P7], but the derivation of the response and the error signal is given in the Appendix of this thesis. The analysis of the remaining error angle, again when the error signal is controlled to zero, indicates that the original reasoning in Publications [P2] and [P3] stays intact. In addition, the publication discusses the current and

voltage measurements for the tracking controller. A simplified controller structure, inspired by the results of [P6], is explained. Experiments using the simplified structure indicate that the test signal frequency and amplitude, as well as the gains of the controller, can be varied at least in a 1:2 range without losing stability in the low-speed region.

Publication [P8]

The tracking controller, as described in Publications [P3] – [P7], is accompanied by a simple voltage-model-based circuit to improve the dynamic response of the system. However, the dynamic performance is only moderate: load torque steps exceeding 50 % of the rated torque may lead to instability. Therefore, the simple model is replaced by a speed-adaptive full-order flux observer in Publication [P8]. The error signal from the tracking controller is used as feedback in the speed-adaptation law in the flux observer, in addition to the feedback from the error in the stator current. Experimental results show that the performance of the speed-adaptive full-order flux observer is improved. The additional feedback stabilizes the regenerating low-speed operation and operation at sustained zero stator frequency. Slow load torque reversals at zero speed were also successfully carried out.

Publication [P9]

The principle of the low-frequency injection method was originally derived for the induction motor. However, the principle can equally well be applied to a non-salient permanent-magnet synchronous motor. Publication [P9] outlines the approach, following that given for the induction motor in Publications [P2] and [P3], and describes the results of simulations of a permanent-magnet synchronous motor, the rotor position of which is estimated using the low-frequency injection method. The results indicate that stable operation in all four quadrants including zero speed can be reached. The selection of the test signal frequency and amplitude, as well as the selection of the controller gains, was studied in the simulations; stable operation was achieved in approximately a 1:2 range for these parameters. Errors up to 20 % in motor parameter estimates were shown to be insignificant.

6 Contribution of This Thesis

The work leading to this thesis was motivated by the difficulty of achieving sustained operation of a speed sensorless induction motor drive close to zero stator frequency. As outlined in Chapter 1, the target for this thesis was to find a simple, yet robust, solution to the problem. The work is based on taking the equation of motion into account, in addition to the equations of the fundamental-wave motor model, and leads to the following contributions:

- It is shown that the response of the system to a low-frequency voltage or current signal injected into the stator winding depends on the direction of the signal relative to the rotor flux direction.
- Based on the aforementioned dependency, a new algorithm for rotor flux angle estimation is proposed and successfully simulated, as well as implemented in a laboratory setup. The algorithm makes sustained zero-frequency operation possible.
- The robustness of the algorithm against errors in the required motor parameter estimates is shown both theoretically and experimentally.
- It is also shown that the algorithm can be combined with a full-order flux observer without losing the steady-state zero-frequency stability and robustness against parameter errors.

This thesis contributes a well-founded method to help in the task of rotor flux angle estimation. Referring to Table 3.2, it is believed that the approach is new.

7 Conclusion

The problem of low-speed operation of speed sensorless induction motor drives is well known. The core of the problem is the difficulty of the rotor flux angle estimation. In this thesis, a new method for the flux angle estimation has been developed. The method yields sensorless control of the motor at low speeds, including operation at zero stator frequency and up to rated load torque, even with considerable errors in the motor parameter estimates.

The method is based on augmenting the fundamental-wave motor model with a simple first-order model of the mechanical dynamics to obtain a model of the electromechanical system. To stimulate the system, a low-frequency ac current signal is added to the flux-producing component of the stator current in the estimated rotor flux reference frame. If there is an error angle between the estimated and actual rotor flux angles, the direction of the current signal differs from that of the rotor flux. Consequently, the motor generates a pulsation of the electromagnetic torque at the signal frequency. The amplitude of the pulsation is proportional to the error angle. If the estimated reference frame is leading the actual one, i.e., if the error angle is positive, the torque pulsation is in phase with the ac current signal, and if the error angle is negative, the pulsation is in opposite phase with the signal.

In systems where the total moment of inertia is not too high, the torque pulsation leads to a speed pulsation at the frequency of the test signal. The speed pulsation is detectable from the back-emf, which can be extracted from the stator voltage. If the error angle is positive, the back-emf pulsation leads the ac current signal in phase, whereas the pulsation lags the current signal for a negative error angle. Demodulating the back-emf pulsation yields an error signal proportional to the error angle, indicating whether the current signal was injected in a direction leading or lagging the rotor flux. The error signal is used to adjust the estimated rotor flux angle to coincide with the actual one. Errors in the motor parameter estimates have almost no influence on the error signal.

The low-frequency signal-injection method has been experimentally validated using a 2.2 kW, four-pole, 400 V, 50 Hz induction motor loaded by a permanent

magnet servo-drive. The frequency of the ac current signal used in the experiments was either 25 Hz or 50 Hz, and the amplitude of the signal used in the experiments was usually 1 A, i.e., about 25 % of the nominal magnetizing current. Stable operation was also recorded when using a 0.5 A, 50 Hz current signal. The signal-injection method was first combined with very primitive versions of a voltage-model-based estimator for the angular frequency of the rotor flux. The error signal was fed into a Proportional-Integral controller, the output of which was added to the voltage-model-based estimate of the angular frequency. The system shows excellent steady-state characteristics at low speeds, and also tolerates considerable errors in the motor parameter estimates.

It is also possible to use the error signal as an additional feedback term in a more advanced flux observer. Experiments using a combination of a speed-adaptive full-order flux observer and the signal-injection method indicate that the steady-state stability and robustness against parameter errors of the full-order observer are improved due to inclusion of the signal-injection method, while the good dynamic performance of the full-order flux observer is retained.

While it is concluded that the targets outlined in Chapter 1 have mostly been reached, some remarks are appropriate. It is clear that the applicability of the method diminishes as the total moment of inertia in the system increases. To compensate that effect, the test signal frequency can be reduced, but since the test signal period should be sufficiently short in respect to the rotor time constant, there is an upper limit to the tolerable moment of inertia. However, it should be noted that in many applications, for example, in lifting, there is often a gear, and the load-side moment of inertia is reduced, as seen from the motor side. Mixing and stirring viscous fluids may provide excellent application areas for the method since the method is not sensitive to viscous friction, and since there should be no concern about the possible vibration caused by the signal injection. Moreover, in these applications, the load torque is smooth. In general, any application demanding sustained operation close to zero frequency may benefit from the method.

On the other hand, several topics for further research can be identified. The mechanical subsystem was modeled as a first-order system in this thesis. Higher-order mechanical systems should also be considered. The effect of possible back-slash in the mechanical coupling of the load may represent a problem with light loads, which should be investigated. Similarly, if the load torque exhibits a spectrum including components interfering with the algorithm, some countermeasures should be devised. In the algorithm presented in this thesis, only the q component of the back-emf response is used. Using the d component in addition could possibly improve the performance. Further, the waveform of the injected current signal could, in principle,

be different from a pure sinusoidal wave. Using a signal with a wider spectrum could possibly improve the dynamic performance of the algorithm. Minimization of the extra losses caused by the injected signal is also a topic for further research. As already pointed out in this thesis, the algorithm can be also applied to non-salient permanent-magnet synchronous motors. Experimental work in this area still needs to be done. Most important, experimental research using induction motors smaller and larger than the 2.2 kW used so far should be conducted, and practical applications, such as lifting, should be tried.

In the author's opinion, the most attractive future for the developed algorithm would be one in which the algorithm is seamlessly combined with another flux observer, helping to improve the low-speed performance if it can, but not causing any harm if it cannot.

References

Abbondanti, A. (1977). Method of flux control in induction motors driven by variable frequency, variable voltage supplies. *Conference Record of the 1977 Annual Meeting of the IEEE Industry Applications Society, IAS 1977*, Los Angeles, CA, 2-6 October, 1977, pp. 177-184.

Aime, M.L., Degner, M.W. and Lorenz, R.D. (1998). Saturation measurements in AC machines using carrier signal injection. *Conference Record of the 1998 IEEE Industry Applications Conference, IAS 1998*, St. Louis, MO, 12-15 October, 1998, Vol. 1, pp. 159-166.

Bauer, F., Heining, H.-D. (1989). Quick response space vector control for a high power three-level-inverter drive system. *Proceedings of 3rd European Conference on Power Electronics and Applications, EPE'89*, Aachen, Germany, 9-12 October, 1989, Vol.1, pp. 417-421.

Blaschke, F. (1972). The principle of field orientation as applied to the new TRANSVEKTOR closed-loop control system for rotating-field machines. *Siemens Review XXXIX (1972*), No 5, pp. 217-220.

Blaschke, F., van der Burgt, J. and Vandenput, A. (1996). Sensorless direct field orientation at zero flux frequency. *Conference Record of the 1996 IEEE Industry Applications Conference, IAS 1996,* San Diego, CA, 6-10 October, 1996, Vol. 1, pp. 189-196.

Blasco-Gimenez, R., Asher, G.M., Sumner, M. and Bradley, K.J. (1996a). Dynamic performance limitations for MRAS based sensorless induction motor drives. Part 1: Stability analysis for the closed loop drive. *IEE Proceedings-Electric Power Applications,* Vol. 143, No. 2, March 1996, pp. 113-122.

Blasco-Gimenez, R., Asher, G.M., Sumner, M. and Bradley, K.J. (1996b). Dynamic performance limitations for MRAS based sensorless induction motor drives. Part 2:

Online parameter tuning and dynamic performance studies. *IEE Proceedings-Electric Power Applications,* Vol. 143, No. 2, March 1996, pp. 123-134.

Bonanno, F., Consoli, A., Raciti, A. and Testa, A. (1997). An innovative direct self-control scheme for induction motor drives. *IEEE Transactions on Power Electronics,* Vol. 12, No. 5, September 1997, pp. 800-806.

Briz, F., Degner, M.W., Diez, A. and Lorenz, R.D. (2001a). Measuring, modeling, and decoupling of saturation-induced saliencies in carrier-signal injection-based sensorless AC drives. *IEEE Transactions on Industry Applications*, Vol. 37, No. 5, September/October 2001, pp. 1356-1364.

Briz, F., Degner, M.W., Diez, A. and Lorenz, R.D. (2002). Static and dynamic behavior of saturation-induced saliencies and their effect on carrier-signal-based sensorless AC drives. *IEEE Transactions on Industry Applications,* Vol. 38, No. 3, May/June 2002, pp. 670-678.

Briz, F., Degner, M.W., Guerrero, J.M. and Diez, A. (2001b). Improving the dynamic performance of carrier signal injection based sensorless AC drives. *Proceedings of the 9th European Conference on Power Electronics and Applications, EPE-2001,* Graz, Austria, 27-29 August, 2001, on CD-ROM.

Briz, F., Diez, A. and Degner, M.W., (2000). Dynamic operation of carrier-signal-injection-based sensorless direct field-oriented ac drives. *IEEE Transactions on Industry Applications,* Vol. 36, No. 5, September/October 2000, pp. 1360-1368.

Caruana, C., Asher, G.M. and Clare, J. (2003). Sensorless vector control at low and zero frequency considering zero-sequence current in delta connected cage induction motors. *Conference Record of the 29th Annual Conference of the IEEE Industrial Electronics Society*, *IECON'03,* Roanoke, VA, 2-6 November, 2003, pp. 1460-1465.

Cilia, J., Asher, G.M., Bradley, K.J. and Sumner, M. (1997). Sensorless position detection for vector-controlled induction motor drives using an asymmetric outer-section cage. *IEEE Transactions on Industry Applications,* Vol. 33, No. 5, September/October 1997, pp. 1162-1169.

Consoli, A., Scarcella, G. and Testa, A. (2000a). A new zero-frequency flux-position detection approach for direct-field-oriented-control drives. *IEEE Transactions on Industry Applications*, Vol. 36, No. 3, May/June 2000, pp. 797-804.

Consoli, A., Scarcella, G., Testa, A. and Lipo, T.A. (2000b). Air-gap flux position estimation of inaccessible neutral induction machines by zero sequence voltage. *Symposium on Power Electronics, Electrical Drives, Automation & Motion, SPEEDAM*, Ischia, Italy, 13-16 June, 2000, pp. B1-1 – B1-6.

De Doncker, R.W. and Novotny, D.W. (1994). The universal field oriented controller. *IEEE Transactions on Industry Applications,* Vol. 30, No. 1, January/February 1994, pp. 92-100.

Degner, M.W. and Lorenz, R.D. (2000). Position estimation in induction machines utilizing rotor bar slot harmonics and carrier-frequency signal injection. *IEEE Transactions on Industry Applications,* Vol. 36, No. 3, May/June 2000, pp. 736-742.

Depenbrock, M., Foerth, C. and Koch, S. (1999). Speed sensorless control of induction motors at very low stator frequencies. *Proceedings of the 8th European Conference on Power Electronics and Applications, EPE'99,* Lausanne, Switzerland, 7-9 September, 1999, on CD-ROM.

Drevensek, D., Zarko, D. and Lipo, T.A. (2002). A study of sensorless control of induction motor at zero speed utilizing high frequency voltage injection. *Proceedings of EPE-PEMC 2002,* Dubrovnik&Cavtat, Croatia, 2002, on CD-ROM.

Ha, J.-I. and Sul, S.-K. (1999). Sensorless field-orientation control of an induction machine by high-frequency signal injection. *IEEE Transactions on Industry Applications,* Vol. 35, No. 1, January/February 1999, pp. 45-51.

Ha, J.-I., Sul, S.-K., Ide, K., Murokita, I. and Sawamura, K. (2000). Physical understanding of high frequency injection method to sensorless drives of an induction machine. *Conference Record of the 2000 IEEE Industry Applications Conference, IAS 2000,* Rome, Italy, 8-12 October, 2000, Vol. 3, pp. 1802-1808.

Harnefors, L. (1998). A comparison between directly parametrised observers and extended Kalman filters for sensorless induction motor drives. *Conference Record of the Seventh International Conference on Power Electonics and Variable Speed Drives,* London, UK, 21-23 September, 1998, pp. 275-280.

Harnefors, L. (2000). Instability phenomena and remedies in sensorless indirect field oriented control. *IEEE Transactions on Power Electronics,* Vol. 15, No. 4, July 2000, pp. 733-743.

Harnefors, L. (2001). Design and analysis of general rotor-flux-oriented vector control systems. *IEEE Transactions on Industrial Electronics,* Vol. 48, No. 2, April 2001, pp. 383-390.

Hillenbrand, F. (1983). A method for determining the speed and rotor flux of the asynchronous machine by measuring the terminal quantities only. *Proceedings of the 3rd IFAC Symposium on Control in Power Electronics and Electrical Drives,* Lausanne, Switzerland, 12-14 September, 1983, pp. 55-62.

Hinkkanen, M. and Luomi, J. (2003). Stabilization of the regenerating mode of full-order flux observers for sensorless induction motors. *Proceedings of the 2003 IEEE International Electric Machines and Drives Conference, IEMDC'03.* Madison, WI, 1-4 June, 2003, pp. 145-150.

Hofmann, H. and Sanders, S.R. (1998). Speed-sensorless vector torque control of induction machines using a two-time-scale approach. *IEEE Transactions on Industry Applications,* Vol. 344, No. 1, January/February 1998, pp. 169-177.

Holtz, J. (2002). Sensorless control of induction motor drives. *Proceedings of the IEEE*, Vol. 90, No. 8, August 2002, pp. 1359-1394.

Holtz, J., Jiang, J. and Pan, H. (1997). Identification of rotor position and speed of standard induction motors at low speed including zero stator frequency. *Proceedings of the 23rd International Conference on Industrial Electronics, Control and Instrumentation, IECON'97,* New Orleans, LA, 9-14 November, 1997, Vol. 2, pp. 971-976.

Hurst, K.D. and Habetler, T.G. (1997). A comparison of spectrum estimation techniques for sensorless speed detection in induction machines. *IEEE Transactions on Industry Applications,* Vol. 33, No. 4, July/August 1997, pp. 898-905.

Hurst, K.D., Habetler, T.G., Griva, G., Profumo, F. and Jansen, P.L. (1995). A self-tuning, closed-loop flux observer for sensorless torque control of standard induction machines. *IEEE Transactions on Power Electronics,* Vol. 12, No. 5, September 1997, pp. 807-815.

Ide, K., Ha, J.-I., Sawamura, M., Iura, H. and Yamamoto, Y. (2002). A novel hybrid speed estimator of flux observer for induction motor drives. *Proceedings of the 2002 IEEE International Symposium on Industrial Electronics, ISIE 2002,* L'Aquila, Italy, 26-29 May, 2002, Vol. 3, pp. 822-827.

Ishida, M. and Iwada, K. (1982). A new slip frequency detector of an induction motor utilizing rotor slot harmonics. *Proceedings of the International Power Semiconductor Conference,* Orlando, FL, 1982, pp. 408-415.

Jansen, P.L. and Lorenz, R.D. (1993). Accuracy limitations of velocity and flux estimation in direct field oriented induction machines. *Conference Record of the 5th European Conference on Power Electronics and Applications, EPE 1993,* Brighton, UK, 13-17 September, 1993, Vol. 4, pp. 312-318.

Jansen, P.L. and Lorenz, R.D. (1994). A physically insightful approach to the design and accuracy assessment of flux observers for field oriented induction machine drives. *IEEE Transactions on Industry Applications*, Vol. 30, No. 1, January/February 1994, pp. 101-110.

Jansen, P.L. and Lorenz, R.D. (1995). Transducerless position and velocity estimation in induction and salient machines. *IEEE Transactions on Industry Applications,* Vol. 31, No. 2, March/April 1995, pp. 240-247.

Jansen, P.L. and Lorenz, R.D. (1996). Transducerless field orientation concepts employing saturation-induced saliencies in induction machines. *IEEE Transactions on Industry Applications*, Vol. 32, No. 6, November/December 1996, pp. 1380-1393.

Jiang, J. and Holtz, J. (1997). High dynamic speed sensorless AC drive with on-line model parameter tuning for steady-state accuracy. *IEEE Transactions on Industrial Electronics,* Vol. 44, No. 2, April 1997, pp. 240-246.

Joetten, R. and Maeder, G. (1983). Control methods for good dynamic performance induction motor drives based on current and voltage as measured quantities. *IEEE Transactions on Industry Applications,* Vol. IA-19, No. 3, pp. 356-363.

Kaku, B., Miyashita, I. and Yasukawa, S. (1998). Novel speed estimation method for induction motor based on extra rotor synchronous current control. *Conference Record of the 29th Annual IEEE Power Electronics Specialists Conference, PESC'98,* Fukuoka, Japan, 17-22 May, 1998, Vol. 1, pp. 852-856.

Kazmierkowski, M.P. and Tunia, H. (1994). *Automatic Control of Converter-Fed Drives.* Elsevier Science Publications B.V., Amsterdam.

Kim, J., Nam, K., Chung, J. and Sunwoo, H. (2003). Sensorless vector control scheme for induction motors based on a stator flux estimator with quadrant error

compensation rule. *IEEE Transactions on Industry Applications*, Vol. 39, No. 2, March/April 2003, pp. 492-503.

Kovács, K. P. and Rácz, I. (1959). *Transiente Vorgänge in Wechselstrommaschinen, Band I, Band II.* Verlag der Ungarischen Akademie der Wissenschaften, Budapest, 1959.

Kubota, H., Sato, I., Tamura, Y., Matsuse, K., Ohta, H. and Hori, Y. (2002). Regenerating-mode low-speed operation of sensorless induction motor drive with adaptive observer. *IEEE Transactions on Industry Applications,* Vol. 38, No. 4, July/August 2002, pp. 1081-1086.

Luenberger, D.G. (1971). An introduction to observers. *IEEE Transactions on Automatic Control.* Vol. AC-16, No. 6, December 1971, pp. 596-602.

Marwali, M.N. and Keyhani, A. (1997). A Comparative study of rotor flux based MRAS and back EMF based MRAS speed estimators for speed sensorless vector control of induction machines. *Conference Record of the 1997 IEEE Industry Applications Conference, IAS 1997,* New Orleans, LA, 5-9 October, 1997, Vol. 1, pp. 160-166.

Moreira, J.C. and Lipo, T.A. (1992). Modeling of saturated AC machines including air gap flux harmonic components. *IEEE Transactions on Industry Applications,* Vol. 28, No. 2, March/April 1992, pp. 343-349.

Moreira, J.C., Lipo, T.A. and Blasko, V. (1991). Simple efficiency maximizer for an adjustable frequency induction motor drive. *IEEE Transactions on Industry Applications,* Vol. 27, No. 5, September/October 1991, pp. 940-946.

Park, R.H. (1929). Two-reaction theory of synchronous machines. Generalized method of analysis – Part I. *Transactions of the AIEE,* Vol. 48, 1929, pp. 716-727.

Peng, F.-Z. and Fukao, T. (1994). Robust speed identification for speed-sensorless vector control of induction motors. *IEEE Transactions on Industry Applications*, Vol. 30, No. 5, September/October 1994, pp. 1234-1240.

Rajashekara, K., Kawamura, A. and Matsuse, K. (Editors) (1996). *Sensorless Control of AC Motor Drives.* IEEE Press, Piscataway, NJ.

Ribeiro, L.A.S., Degner, M.W., Briz, F. and Lorenz, R.D. (1998). Comparison of carrier signal voltage and current injection for the estimation of flux angle or rotor

position. *Conference Record of the 1998 IEEE Industry Applications Conference, IAS 1998*, St. Louis, MO, 12-15 October, 1998, Vol. 1, pp. 452-459.

Schauder, C. (1992). Adaptive speed identification for vector control of induction motors without rotational transducers. *IEEE Transactions on Industry Applications*, Vol. 28, No. 5, September/October 1992, pp. 1054-1061.

Schroedl, M. (1992). Sensorless control of induction motors at low speed and standstill. *Conference Record of the International Conference on Electrical Machines, ICEM´92*, Manchester, 1992, pp. 863-867.

Sng, E.K.K, Liew, A.-C. and Lipo, T.A. (1998). New observer-based DFO scheme for speed sensorless field-oriented drives for low–zero-speed operation. *IEEE Transactions on Power Electronics*, Vol. 13, No. 5, September 1998, pp. 959-968.

Staines, C.S., Asher, G.M. and Bradley, K.J. (1999). A periodic burst injection method for deriving rotor position in saturated cage-salient induction motors without a shaft encoder. *IEEE Transactions on Industry Applications*, Vol. 35, No. 4, July/August 1999, pp. 851-858.

Stanley, H.C. (1938). An analysis of the induction machine. *Transactions of the AIEE*, Vol. 57, 1938, pp. 751-755.

Tajima, H. and Hori, Y. (1993). Speed sensorless field-orientation control of the induction machine. *IEEE Transactions on Industry Applications*, Vol. 29, No. 1, January/February 1993, pp. 175-180.

Takeshita, T., Nagatoshi, Y. and Matsui, N. (2002). Sensorless vector control of induction motor at zero frequency. *Proceedings of the 2002 Power Conversion Conference, PCC 2002,* Osaka, Japan, 2-5 April, 2002, Vol. 2, pp. 510-515.

Teodorescu, R., Bech, M., Blaabjerg, F. and Pedersen, J.K. (2000). Flexible drive systems laboratory – a modern teaching facility in electrical drives at Aalborg University. *Proceedings of 2000 IEEE Nordic Workshop on Power and Industrial Electronics – NORPIE/2000*, Aalborg, Denmark, 13-16 June 2000, pp. 42-46.

Teske, N., Asher, G.M., Sumner, M. and Bradley, K.J. (2000). Suppression of saturation saliency effects for the sensorless position control of induction motor drives under loaded conditions. *IEEE Transactions on Industrial Electronics,* Vol. 47, No. 5, October 2000, pp. 1142-1150.

Teske, N., Asher, G.M., Bradley, K.J. and Sumner, M. (2001a). Analysis and suppression of inverter clamping saliency in sensorless position controlled induction machine drives. *Conference Record of the 2001 IEEE Industry Applications Conference, IAS 2001,* Chicago, Illinois, September 30 – October 4, 2001, pp. 2629-2636.

Teske, N., Asher, G.M., Sumner, M. and Bradley, K.J. (2001b). Encoderless position estimation for symmetric cage induction machines under loaded conditions. *IEEE Transactions on Industry Applications*, Vol. 37, No. 6, November/December 2001, pp. 1793-1800.

Verghese, G.C. and Sanders, S.R. (1988). Observers for flux estimation in induction machines. *IEEE Transactions on Industrial Electronics,* Vol. 35, No. 1, February 1988, pp. 85-94.

Wolbank, T.M., Woehrnschimmel, R. and Machl, J.L. (2002a). Slot geometry – an important design parameter for zero speed sensorless control of standard induction machines. *Proceedings of EPE-PEMC 2002,* Cavtat, Croatia, 9-11 September, 2002, on CD-ROM.

Wolbank, T.M., Wöhrnschimmel, R. and Hauser, H. (2002b). Transient simulation of lamination material properties in electrical machines. *IEEE Transactions on Industrial Electronics,* Vol. 49, No. 3, June 2002, pp. 607-612.

Wolbank, T. and Haidvogl, B. (2000). Evaluation of the influence of design and operation of standard induction motors on sensorless control schemes utilising saliencies in the transient electrical behaviour. *2000 IEEE 31st Annual Power Electronics Specialists Conference, PESC'00*, Galway, Ireland, 16-23 June, 2000, Vol. 2, pp. 903-908.

Åström, K.J. and Wittenmark, B. (1995). *Adaptive Control* (2nd edition). Addison-Wesley Publishing Company, Reading, MA.

Åström, K.J. and Wittenmark, B. (1997). *Computer-Controlled Systems – Theory and Design* (3rd edition). Prentice-Hall Inc., Upper Saddle River, NJ.

Appendix

Error signal derivation

Perturbations around a quiescent operating point

An induction motor is assumed to operate in steady state at a quiescent operating point. The space vector of the quiescent stator current, expressed in a reference frame attached to the rotor flux linkage is

$$\underline{i}_{\mathrm{s0}} = i_{\mathrm{d0}} + \mathrm{j} i_{\mathrm{q0}} \,. \tag{A.1}$$

The quiescent rotor flux linkage is ψ_{R0}, and the quiescent electromagnetic torque is

$$T_{\mathrm{e0}} = \frac{3p}{2} \psi_{\mathrm{R0}} i_{\mathrm{q0}} \,. \tag{A.2}$$

The load torque is assumed to be $T_{\mathrm{L}} = T_{\mathrm{e0}}$. The quiescent angular speed of the shaft, in electrical radians per second, is ω_{m0}. The space vector of the quiescent back-emf is

$$\underline{e}_0 = (1/\tau_{\mathrm{r}} - \mathrm{j}\omega_{\mathrm{m0}})\psi_{\mathrm{R0}} \,, \tag{A.3}$$

where τ_{r} is the rotor time constant. If there is a perturbation $T_{\mathrm{ec}}(s)$ in the electromagnetic torque, the torque is $T_{\mathrm{e}} = T_{\mathrm{e0}} + T_{\mathrm{ec}}(s)$. The speed will react to the torque perturbation: $\omega_{\mathrm{m}} = \omega_{\mathrm{m0}} + \omega_{\mathrm{mc}}(s)$. The speed perturbation $\omega_{\mathrm{mc}}(s)$ is given by the equation of motion

$$\omega_{\mathrm{mc}}(s) = \frac{p}{b + sJ} T_{\mathrm{ec}}(s) \,, \tag{A.4}$$

where p is the number of pole pairs, b the coefficient of viscous friction and J the total moment of inertia. Due to the speed perturbation, the back-emf will also be perturbed to $\underline{e} = \underline{e}_0 + \underline{e}_{\mathrm{c}}(s)$.

In the following, expressions for the back-emf response $\underline{e}_{\mathrm{c}}(s) = e_{\mathrm{cd}}(s) + \mathrm{j}e_{\mathrm{cq}}(s)$ are derived, assuming the torque perturbation $T_{\mathrm{ec}}(s)$ to be caused by stator current perturbations $i_{\mathrm{cq}}(s)$ and $i_{\mathrm{cd}}(s)$, given respectively in the q and d directions of the rotor flux reference frame. Based on the result, a pair of current perturbations is used to give rise to back-emf response in an estimated rotor flux reference frame. Finally, an error signal approximately proportional to the error angle between the estimated and actual rotor flux angles is derived from the back-emf response.

Perturbation in stator current q component

If there is a perturbation in the q component of the stator current, the stator current is $\underline{i}_{\mathrm{s}} = i_{\mathrm{d0}} + \mathrm{j}\Big[i_{\mathrm{q0}} + i_{\mathrm{cq}}(s)\Big]$. The rotor flux linkage is not affected by the perturbation: $\psi_{\mathrm{R}} = \psi_{\mathrm{R0}}$. The electromagnetic torque will be affected:

$$T_{\mathrm{e}} = \frac{3p}{2}\psi_{\mathrm{R0}}\Big[i_{\mathrm{q0}} + i_{\mathrm{cq}}(s)\Big]. \tag{A.5}$$

Since it is assumed that $T_{\mathrm{L}} = T_{\mathrm{e0}}$, the perturbation of the net torque will be

$$T_{\mathrm{ec}}(s) = T_{\mathrm{e}} - T_{\mathrm{L}} = \frac{3p}{2}\psi_{\mathrm{R0}} i_{\mathrm{cq}}(s). \tag{A.6}$$

Hence the speed will be perturbed around its quiescent value:

$$\omega_{\mathrm{m}} = \omega_{\mathrm{m0}} + \frac{3p^2\psi_{\mathrm{R0}}}{2b}\frac{i_{\mathrm{cq}}(s)}{1 + s\tau_{\mathrm{m}}}, \tag{A.7}$$

where the mechanical time constant is $\tau_{\mathrm{m}} = J/b$. The speed perturbation

$$\omega_{\mathrm{mc}}(s) = \frac{3p^2\psi_{\mathrm{R0}}}{2b}\frac{i_{\mathrm{cq}}(s)}{1 + s\tau_{\mathrm{m}}} \tag{A.8}$$

affects the back-emf

$$\underline{e} = \underbrace{\left(\frac{1}{\tau_{\mathrm{r}}} - \mathrm{j}\omega_{\mathrm{m0}}\right)\psi_{\mathrm{R0}}}_{=\underline{e}_0} - \underbrace{\mathrm{j}\frac{3p^2\psi_{\mathrm{R0}}^2}{2b}\frac{i_{\mathrm{cq}}(s)}{1 + s\tau_{\mathrm{m}}}}_{=\underline{e}_{\mathrm{c}}(s)}. \tag{A.9}$$

The transfer functions from the q-directed current perturbation to the d and q components of the back-emf can thus be defined as

$$G_{\mathrm{cqq}}(s) = \frac{e_{\mathrm{cq}}(s)}{i_{\mathrm{cq}}(s)} = -\frac{3p^2\psi_{\mathrm{R0}}^2}{2b}\frac{1}{1 + s\tau_{\mathrm{m}}} \tag{A.10}$$

and

$$G_{\mathrm{cqd}}(s) = \frac{e_{\mathrm{cd}}(s)}{i_{\mathrm{cq}}(s)} = 0. \tag{A.11}$$

Perturbation in stator current d component

A perturbation in the d component of the stator current gives $\underline{i}_\mathrm{s} = i_\mathrm{d0} + i_\mathrm{cd}(s) + \mathrm{j}i_\mathrm{q0}$. Now the rotor flux linkage is affected by the perturbation:

$$\psi_\mathrm{R} = \psi_\mathrm{R0} + \frac{L_\mathrm{dyn} i_\mathrm{cd}(s)}{1 + s\tau_\mathrm{rc}}, \tag{A.12}$$

where the rotor time constant is $\tau_\mathrm{rc} = L_\mathrm{dyn} / R_\mathrm{Rc}$. The dynamic inductance $L_\mathrm{dyn} = \Delta\psi_\mathrm{R} / \Delta i_\mathrm{d}$ is evaluated at the quiescent flux linkage level ψ_R0, and R_Rc is the rotor resistance evaluated at the frequency of the perturbation. The perturbation in the rotor flux linkage causes a perturbation in the electromagnetic torque (when $i_\mathrm{q0} \neq 0$):

$$T_\mathrm{e} = \frac{3p}{2}\left[\psi_\mathrm{R0} + \frac{L_\mathrm{dyn} i_\mathrm{cd}(s)}{1 + s\tau_\mathrm{rc}}\right] i_\mathrm{q0}. \tag{A.13}$$

Since $T_\mathrm{L} = T_\mathrm{e0}$, the net torque will be

$$T_\mathrm{ec}(s) = T_\mathrm{e} - T_\mathrm{L} = \frac{3p}{2}\frac{L_\mathrm{dyn} i_\mathrm{cd}(s)}{1 + s\tau_\mathrm{rc}} i_\mathrm{q0}. \tag{A.14}$$

The speed perturbation is thus

$$\omega_\mathrm{mc}(s) = \frac{3p^2 L_\mathrm{dyn} i_\mathrm{q0}}{2b} \frac{i_\mathrm{cd}(s)}{(1 + s\tau_\mathrm{m})(1 + s\tau_\mathrm{rc})} \tag{A.15}$$

and the back-emf will be

$$\begin{aligned}\underline{e} = &\underbrace{\left(\frac{1}{\tau_\mathrm{r}} - \mathrm{j}\omega_\mathrm{m0}\right)\psi_\mathrm{R0}}_{=\underline{e}_0} \\ &+ \underbrace{\left(\frac{1}{\tau_\mathrm{rc}} - \mathrm{j}\omega_\mathrm{m0}\right) L_\mathrm{dyn} \frac{i_\mathrm{cd}(s)}{1 + s\tau_\mathrm{rc}} - \mathrm{j}\frac{3p^2 L_\mathrm{dyn} i_\mathrm{q0}}{2b} \frac{i_\mathrm{cd}(s)}{(1 + s\tau_\mathrm{m})(1 + s\tau_\mathrm{rc})}\left[\psi_\mathrm{R0} + L_\mathrm{dyn} \frac{i_\mathrm{cd}(s)}{1 + s\tau_\mathrm{rc}}\right]}_{=\underline{e}_\mathrm{c}(s)}\end{aligned} \tag{A.16}$$

The transfer functions from the d-directed current perturbation to the d and q components in the back-emf can be defined as

$$G_\mathrm{cdd}(s) = \frac{e_\mathrm{cd}(s)}{i_\mathrm{cd}(s)} = \frac{R_\mathrm{Rc}}{1 + s\tau_\mathrm{rc}} \tag{A.17}$$

and

$$G_{\mathrm{cdq}}(s)=\frac{e_{\mathrm{cq}}(s)}{i_{\mathrm{cd}}(s)}\approx \underbrace{-\frac{\omega_{\mathrm{m0}}L_{\mathrm{dyn}}}{1+s\tau_{\mathrm{rc}}}}_{\substack{\text{due to the change}\\ \text{in flux amplitude}}} \underbrace{-\frac{3p^2L_{\mathrm{dyn}}i_{\mathrm{q0}}\psi_{\mathrm{R0}}}{2b}\frac{1}{(1+s\tau_{\mathrm{m}})(1+s\tau_{\mathrm{rc}})}}_{\text{due to the change in speed}}, \tag{A.18}$$

where the approximation $\psi_{\mathrm{R0}}+L_{\mathrm{dyn}}\dfrac{i_{\mathrm{cd}}(s)}{1+s\tau_{\mathrm{rc}}}\approx\psi_{\mathrm{R0}}$ was used.

Simultaneous perturbations in stator current d and q components

Simultaneous current perturbations both in the d and q directions are assumed as $i_{\mathrm{cd}}(t)=\sqrt{2}I_{\mathrm{cd}}\cos(\omega_{\mathrm{c}}t)$ and $i_{\mathrm{cq}}(t)=\sqrt{2}I_{\mathrm{cq}}\cos(\omega_{\mathrm{c}}t+\varphi)$, and their phasors are defined as $\underline{I}_{\mathrm{cd}}=I_{\mathrm{cd}}\angle 0$ and $\underline{I}_{\mathrm{cq}}=I_{\mathrm{cq}}\angle\varphi$, respectively. The response in the back-emf to the current perturbations is given by the phasor equation

$$\begin{bmatrix}\underline{E}_{\mathrm{cd}}\\ \underline{E}_{\mathrm{cq}}\end{bmatrix}=\begin{bmatrix}\underline{Z}_{\mathrm{cdd}} & \underline{Z}_{\mathrm{cqd}}\\ \underline{Z}_{\mathrm{cdq}} & \underline{Z}_{\mathrm{cqq}}\end{bmatrix}\begin{bmatrix}\underline{I}_{\mathrm{cd}}\\ \underline{I}_{\mathrm{cq}}\end{bmatrix}. \tag{A.19}$$

The impedances of the equation are obtained from the corresponding transfer functions (A.10-11) and (A.17-18), by a substitution $s=\mathrm{i}\omega_{\mathrm{c}}$:

$$\underline{Z}_{\mathrm{cdd}}=G_{\mathrm{cdd}}(\mathrm{i}\omega_{\mathrm{c}})=a_1+\mathrm{i}b_1 \tag{A.20a}$$

$$\underline{Z}_{\mathrm{cdq}}=G_{\mathrm{cdq}}(\mathrm{i}\omega_{\mathrm{c}})=a_2+\mathrm{i}b_2 \tag{A.20b}$$

$$\underline{Z}_{\mathrm{cqd}}=G_{\mathrm{cqd}}(\mathrm{i}\omega_{\mathrm{c}})=0 \tag{A.20c}$$

$$\underline{Z}_{\mathrm{cqq}}=G_{\mathrm{cqq}}(\mathrm{i}\omega_{\mathrm{c}})=a_3+\mathrm{i}b_{13}, \tag{A.20d}$$

where the constants are

$$a_1=\frac{R_{\mathrm{Rc}}}{1+\omega_{\mathrm{c}}^2\tau_{\mathrm{rc}}^2} \qquad b_1=-\frac{\omega_{\mathrm{c}}L_{\mathrm{dyn}}}{1+\omega_{\mathrm{c}}^2\tau_{\mathrm{rc}}^2}$$

$$a_2=-\frac{\omega_{\mathrm{m0}}L_{\mathrm{dyn}}}{1+\omega_{\mathrm{c}}^2\tau_{\mathrm{rc}}^2}-\frac{3p^2L_{\mathrm{dyn}}i_{\mathrm{q0}}\psi_{\mathrm{R0}}(1-\omega_{\mathrm{c}}^2\tau_{\mathrm{rc}}\tau_{\mathrm{m}})}{2b(1+\omega_{\mathrm{c}}^2\tau_{\mathrm{m}}^2)(1+\omega_{\mathrm{c}}^2\tau_{\mathrm{rc}}^2)} \qquad b_2=\frac{\omega_{\mathrm{c}}\tau_{\mathrm{rc}}\omega_{\mathrm{m0}}L_{\mathrm{dyn}}}{1+\omega_{\mathrm{c}}^2\tau_{\mathrm{rc}}^2}+\frac{3p^2L_{\mathrm{dyn}}i_{\mathrm{q0}}\psi_{\mathrm{R0}}\omega_{\mathrm{c}}(\tau_{\mathrm{rc}}+\tau_{\mathrm{m}})}{2b(1+\omega_{\mathrm{c}}^2\tau_{\mathrm{m}}^2)(1+\omega_{\mathrm{c}}^2\tau_{\mathrm{rc}}^2)}$$

$$a_3=-\frac{3p^2\psi_{\mathrm{R0}}^2}{2b(1+\omega_{\mathrm{c}}^2\tau_{\mathrm{m}}^2)} \qquad b_3=\frac{\omega_{\mathrm{c}}\tau_{\mathrm{m}}3p^2\psi_{\mathrm{R0}}^2}{2b(1+\omega_{\mathrm{c}}^2\tau_{\mathrm{m}}^2)}.$$

Cancellation of torque oscillation

The d-directed current perturbation causes oscillation in the rotor flux, and, if $i_{\mathrm{q}0} \neq 0$, this oscillation causes an oscillation in the torque. To eliminate the torque oscillation, the q-directed perturbation of the stator current can be selected suitably, as shown next. The stator current is

$$\underline{i}_{\mathrm{s}} = i_{\mathrm{d}0} + i_{\mathrm{cd}}(s) + \mathrm{j}\Big[i_{\mathrm{q}0} + i_{\mathrm{cq}}(s)\Big]. \tag{A.21}$$

The rotor flux linkage is given by (A.12), and the electromagnetic torque is

$$T_{\mathrm{e}} = \frac{3p}{2}\left[\psi_{\mathrm{R}0} + \frac{L_{\mathrm{dyn}} i_{\mathrm{cd}}(s)}{1+s\tau_{\mathrm{rc}}}\right]\Big[i_{\mathrm{q}0} + i_{\mathrm{cq}}(s)\Big]. \tag{A.22}$$

Assuming again the load torque to equal the quiescent electromagnetic torque, the net torque is

$$T_{\mathrm{ec}}(s) = T_{\mathrm{e}} - T_{\mathrm{L}} = \frac{3p}{2}\left[\frac{L_{\mathrm{dyn}} i_{\mathrm{cd}}(s)}{1+s\tau_{\mathrm{rc}}} i_{\mathrm{q}0} + \psi_{\mathrm{R}0} i_{\mathrm{cq}}(s) + \frac{L_{\mathrm{dyn}} i_{\mathrm{cd}}(s) i_{\mathrm{cq}}(s)}{1+s\tau_{\mathrm{rc}}}\right]. \tag{A.23}$$

There will be no torque oscillation if $T_{\mathrm{ec}}(s) = 0$, which is approximately satisfied if the q and d components of the stator current perturbation are related by

$$i_{\mathrm{cq}}(s) \approx \frac{-L_{\mathrm{dyn}} i_{\mathrm{q}0}}{\psi_{\mathrm{R}0}\big(1+s\tau_{\mathrm{rc}}\big)} i_{\mathrm{cd}}(s). \tag{A.24}$$

If the d-directed current signal is in time domain $i_{\mathrm{cd}}(t) = \sqrt{2} I_{\mathrm{cd}} \cos\big(\omega_{\mathrm{c}} t\big)$, the phasor of the q-directed current signal should be

$$\underline{I}_{\mathrm{cq}} = \frac{-L_{\mathrm{dyn}} i_{\mathrm{q}0}}{\psi_{\mathrm{R}0}\big(1+\mathrm{i}\omega_{\mathrm{c}}\tau_{\mathrm{rc}}\big)} \underline{I}_{\mathrm{cd}}. \tag{A.25}$$

In the following, estimates $\hat{\tau}_{\mathrm{rc}}$ and $\hat{L}_{\mathrm{dyn}}$ and reference values $i_{\mathrm{q}0}^{\mathrm{ref}}$ and $\psi_{\mathrm{R}0}^{\mathrm{ref}}$ are used, so that $\underline{I}_{\mathrm{cq}} = \underline{C}\underline{I}_{\mathrm{cd}}$, where $\underline{C} = a_4 + \mathrm{i}b_4$ with

$$a_4 = \frac{-\hat{L}_{\mathrm{dyn}} i_{\mathrm{q}0}^{\mathrm{ref}}}{\psi_{\mathrm{R}0}^{\mathrm{ref}}\left(1+\omega_{\mathrm{c}}^2\hat{\tau}_{\mathrm{rc}}^2\right)} \text{ and } b_4 = \frac{\hat{L}_{\mathrm{dyn}} i_{\mathrm{q}0}^{\mathrm{ref}} \omega_{\mathrm{c}}\hat{\tau}_{\mathrm{rc}}}{\psi_{\mathrm{R}0}^{\mathrm{ref}}\left(1+\omega_{\mathrm{c}}^2\hat{\tau}_{\mathrm{rc}}^2\right)}.$$

The time domain expression of the q-directed current perturbation is

$$i_{\mathrm{cq}}(t) = \sqrt{2} C I_{\mathrm{cd}} \cos(\omega_{\mathrm{c}} t + \varphi), \tag{A.26}$$

where

$$C = \frac{\hat{L}_{\mathrm{dyn}} i_{\mathrm{q}0}^{\mathrm{ref}}}{\psi_{\mathrm{R}0}^{\mathrm{ref}}\sqrt{1+\omega_{\mathrm{c}}^2\hat{\tau}_{\mathrm{rc}}^2}} \text{ and } \varphi = \pi/2 + \tan^{-1}(1/\omega_{\mathrm{c}}\hat{\tau}_{\mathrm{r}}).$$

Perturbations and response in the estimated rotor flux reference frame

The angle of the d axis of the estimated rotor flux reference frame is $\hat{\theta}_1$, and it may be misaligned relative to θ_1, the angle of the actual rotor flux. The error angle is defined by $\varepsilon = \hat{\theta}_1 - \theta_1$. Simultaneous current perturbations are given in the d and q directions in the estimated rotor flux reference frame as $i^{\varepsilon}_{\mathrm{cd}}(t) = \sqrt{2} I^{\varepsilon}_{\mathrm{cd}} \cos(\omega_{\mathrm{c}} t)$ and $i^{\varepsilon}_{\mathrm{cq}}(t) = \sqrt{2} I^{\varepsilon}_{\mathrm{cq}} \cos(\omega_{\mathrm{c}} t + \varphi)$, having phasors $\underline{I}^{\varepsilon}_{\mathrm{cd}} = I^{\varepsilon}_{\mathrm{cd}} \angle 0$ and $\underline{I}^{\varepsilon}_{\mathrm{cq}} = I^{\varepsilon}_{\mathrm{cq}} \angle \varphi$, respectively. The back-emf response, as evaluated in the estimated reference frame, can be found with the help of the transformations

$$\begin{bmatrix} \underline{I}_{\mathrm{cd}} \\ \underline{I}_{\mathrm{cq}} \end{bmatrix} = \begin{bmatrix} \cos\varepsilon & -\sin\varepsilon \\ \sin\varepsilon & \cos\varepsilon \end{bmatrix} \begin{bmatrix} \underline{I}^{\varepsilon}_{\mathrm{cd}} \\ \underline{I}^{\varepsilon}_{\mathrm{cq}} \end{bmatrix} \tag{A.27a}$$

and

$$\begin{bmatrix} \underline{E}^{\varepsilon}_{\mathrm{cd}} \\ \underline{E}^{\varepsilon}_{\mathrm{cq}} \end{bmatrix} = \begin{bmatrix} \cos\varepsilon & \sin\varepsilon \\ -\sin\varepsilon & \cos\varepsilon \end{bmatrix} \begin{bmatrix} \underline{E}_{\mathrm{cd}} \\ \underline{E}_{\mathrm{cq}} \end{bmatrix} \tag{A.27b}$$

which, together with (A.19), lead to

$$\begin{bmatrix} \underline{E}^{\varepsilon}_{\mathrm{cd}} \\ \underline{E}^{\varepsilon}_{\mathrm{cq}} \end{bmatrix} = \begin{bmatrix} \underline{Z}^{\varepsilon}_{\mathrm{cdd}} & \underline{Z}^{\varepsilon}_{\mathrm{cqd}} \\ \underline{Z}^{\varepsilon}_{\mathrm{cdq}} & \underline{Z}^{\varepsilon}_{\mathrm{cqq}} \end{bmatrix} \begin{bmatrix} \underline{I}^{\varepsilon}_{\mathrm{cd}} \\ \underline{I}^{\varepsilon}_{\mathrm{cq}} \end{bmatrix}, \tag{A.28}$$

where the impedances are

$$\underline{Z}^{\varepsilon}_{\mathrm{cdd}} = \underline{Z}_{\mathrm{cdd}} \cos^2\varepsilon + \underline{Z}_{\mathrm{cdq}} \cos\varepsilon \sin\varepsilon + \underline{Z}_{\mathrm{cqd}} \cos\varepsilon \sin\varepsilon + \underline{Z}_{\mathrm{cqq}} \sin^2\varepsilon \tag{A.29a}$$

$$\underline{Z}^{\varepsilon}_{\mathrm{cqd}} = -\underline{Z}_{\mathrm{cdd}} \cos\varepsilon \sin\varepsilon - \underline{Z}_{\mathrm{cdq}} \sin^2\varepsilon + \underline{Z}_{\mathrm{cqd}} \cos^2\varepsilon + \underline{Z}_{\mathrm{cqq}} \cos\varepsilon \sin\varepsilon \tag{A.29b}$$

$$\underline{Z}^{\varepsilon}_{\mathrm{cdq}} = -\underline{Z}_{\mathrm{cdd}} \cos\varepsilon \sin\varepsilon + \underline{Z}_{\mathrm{cdq}} \cos^2\varepsilon - \underline{Z}_{\mathrm{cqd}} \sin^2\varepsilon + \underline{Z}_{\mathrm{cqq}} \cos\varepsilon \sin\varepsilon \tag{A.29c}$$

$$\underline{Z}^{\varepsilon}_{\mathrm{cqq}} = \underline{Z}_{\mathrm{cdd}} \sin^2\varepsilon - \underline{Z}_{\mathrm{cdq}} \cos\varepsilon \sin\varepsilon - \underline{Z}_{\mathrm{cqd}} \cos\varepsilon \sin\varepsilon + \underline{Z}_{\mathrm{cqq}} \cos^2\varepsilon . \tag{A.29d}$$

Error signal

When the phasors of the current signals in the estimated rotor flux reference frame are $\underline{I}^{\varepsilon}_{\mathrm{cd}} = I^{\varepsilon}_{\mathrm{cd}} \angle 0$ and $\underline{I}^{\varepsilon}_{\mathrm{cq}} = \underline{C} \underline{I}^{\varepsilon}_{\mathrm{cd}}$, the response in the q-component of the back-emf is, according to (A.28),

$$\underline{E}^{\varepsilon}_{\mathrm{cq}} = \underline{Z}^{\varepsilon}_{\mathrm{cdq}} \underline{I}^{\varepsilon}_{\mathrm{cd}} + \underline{Z}^{\varepsilon}_{\mathrm{cqq}} \underline{I}^{\varepsilon}_{\mathrm{cq}} = (\underline{Z}^{\varepsilon}_{\mathrm{cdq}} + \underline{Z}^{\varepsilon}_{\mathrm{cqq}} \underline{C}) \underline{I}^{\varepsilon}_{\mathrm{cd}} \tag{A.30}$$

which can further be written as

$$\underline{E}^{\varepsilon}_{\mathrm{cq}} = (A + \mathrm{i}B) \underline{I}^{\varepsilon}_{\mathrm{cd}} \tag{A.31}$$

with the constants

$$A = (-a_1 + a_3 - a_2 a_4 + b_2 b_4)\cos\varepsilon\sin\varepsilon + (a_2 + a_3 - b_3 b_4)\cos^2\varepsilon + \left(a_1 a_4 - b_1 b_4\right)\sin^2\varepsilon$$

and

$$B = (-b_1 + b_3 - a_2 b_4 - b_2 a_4)\cos\varepsilon\sin\varepsilon + (b_2 + a_3 b_4 + b_3 a_4)\cos^2\varepsilon + \left(a_1 b_4 + b_1 a_4\right)\sin^2\varepsilon$$

The response is in time domain

$$e_{\mathrm{cq}}^{\varepsilon}(t) = \sqrt{2} I_{\mathrm{cd}}^{\varepsilon}\left[A\cos(\omega_{\mathrm{c}} t) - B\sin(\omega_{\mathrm{c}} t)\right]. \tag{A.32}$$

If the back-emf response is demodulated according to

$$f_{\varepsilon}(t) = \left[e_{\mathrm{cq}}^{\varepsilon}(t) + \frac{\omega_{\mathrm{c}}\hat{\tau}_{\mathrm{rc}}\hat{\omega}_{\mathrm{m0}}\hat{L}_{\mathrm{dyn}}}{1+\omega_{\mathrm{c}}^2\hat{\tau}_{\mathrm{rc}}^2}\sqrt{2} I_{\mathrm{cd}}^{\varepsilon}\sin\left(\omega_{\mathrm{c}} t\right)\right]\sin\left(\omega_{\mathrm{c}} t\right) \tag{A.33}$$

and $f_{\varepsilon}(t)$ is low-pass filtered, the error signal obtained is:

$$\begin{aligned}
F_{\varepsilon} = &\left\{\frac{\omega_{\mathrm{c}}\hat{\tau}_{\mathrm{rc}}\hat{\omega}_{\mathrm{m0}}\hat{L}_{\mathrm{dyn}}}{1+\omega_{\mathrm{c}}^2\hat{\tau}_{\mathrm{rc}}^2} - \cos\varepsilon\sin\varepsilon\left[\frac{\omega_{\mathrm{c}} L_{\mathrm{dyn}}}{1+\omega_{\mathrm{c}}^2\tau_{\mathrm{rc}}^2} + \frac{\omega_{\mathrm{c}}\tau_{\mathrm{m}} 3p^2\psi_{\mathrm{R0}}^2}{2b\left(1+\omega_{\mathrm{c}}^2\tau_{\mathrm{m}}^2\right)}\right.\right. \\
&+\left.\left(\frac{\left(\tau_{\mathrm{rc}}+\hat{\tau}_{\mathrm{rc}}\right)\omega_{\mathrm{m0}} L_{\mathrm{dyn}}}{1+\omega_{\mathrm{c}}^2\tau_{\mathrm{rc}}^2} + \frac{3p^2\psi_{\mathrm{R0}} L_{\mathrm{dyn}} i_{\mathrm{q0}}\left(\tau_{\mathrm{rc}}+\hat{\tau}_{\mathrm{rc}}+\tau_{\mathrm{m}}-\omega_{\mathrm{c}}^2\tau_{\mathrm{rc}}\hat{\tau}_{\mathrm{rc}}\tau_{\mathrm{m}}\right)}{2b\left(1+\omega_{\mathrm{c}}^2\tau_{\mathrm{m}}^2\right)\left(1+\omega_{\mathrm{c}}^2\tau_{\mathrm{rc}}^2\right)}\right)\frac{\omega_{\mathrm{c}}\hat{L}_{\mathrm{dyn}} i_{\mathrm{q0}}^{\mathrm{ref}}}{\psi_{\mathrm{R0}}^{\mathrm{ref}}\left(1+\omega_{\mathrm{c}}^2\hat{\tau}_{\mathrm{rc}}^2\right)}\right] \\
&-\cos^2\varepsilon\left[\frac{\omega_{\mathrm{c}}\tau_{\mathrm{rc}}\omega_{\mathrm{m0}} L_{\mathrm{dyn}}}{1+\omega_{\mathrm{c}}^2\tau_{\mathrm{rc}}^2} + \frac{3p^2\psi_{\mathrm{R0}} L_{\mathrm{dyn}} i_{\mathrm{q0}}\omega_{\mathrm{c}}\left(\tau_{\mathrm{rc}}+\tau_{\mathrm{m}}\right)}{2b\left(1+\omega_{\mathrm{c}}^2\tau_{\mathrm{m}}^2\right)\left(1+\omega_{\mathrm{c}}^2\tau_{\mathrm{rc}}^2\right)} - \frac{3p^2\psi_{\mathrm{R0}}^2\hat{L}_{\mathrm{dyn}} i_{\mathrm{q0}}^{\mathrm{ref}}\omega_{\mathrm{c}}\left(\hat{\tau}_{\mathrm{rc}}+\tau_{\mathrm{m}}\right)}{2b\psi_{\mathrm{R0}}^{\mathrm{ref}}\left(1+\omega_{\mathrm{c}}^2\tau_{\mathrm{m}}^2\right)\left(1+\omega_{\mathrm{c}}^2\hat{\tau}_{\mathrm{rc}}^2\right)}\right] \\
&\left.\left.-\sin^2\varepsilon\frac{\hat{L}_{\mathrm{dyn}} i_{\mathrm{q0}}^{\mathrm{ref}}\omega_{\mathrm{c}}\left(R_{\mathrm{Rc}}\hat{\tau}_{\mathrm{rc}}+L_{\mathrm{dyn}}\right)}{\psi_{\mathrm{R0}}^{\mathrm{ref}}\left(1+\omega_{\mathrm{c}}^2\tau_{\mathrm{rc}}^2\right)\left(1+\omega_{\mathrm{c}}^2\hat{\tau}_{\mathrm{rc}}^2\right)}\right\}\frac{I_{\mathrm{cd}}^{\varepsilon}}{\sqrt{2}}
\end{aligned} \tag{A.34}$$

The result (A.34) can be verified by inserting (A.32) into (A.33) and expanding the constants A and B with the expressions for a_1 to a_4 and b_1 to b_4. In (A.34), terms approximately proportional to ω_{c}^{-3} and smaller can be disregarded. If the error angle $\varepsilon \ll 1$, the approximations $\sin\varepsilon \approx \varepsilon$ and $\cos\varepsilon \approx 1$ can be adopted. Thus (A.34) simplifies to

$$F_{\varepsilon} \approx \left[\frac{\omega_{\mathrm{c}}\hat{\tau}_{\mathrm{rc}}\hat{\omega}_{\mathrm{m0}}\hat{L}_{\mathrm{dyn}}}{1+\omega_{\mathrm{c}}^2\hat{\tau}_{\mathrm{rc}}^2} - \frac{\omega_{\mathrm{c}}\tau_{\mathrm{rc}}\omega_{\mathrm{m0}} L_{\mathrm{dyn}}}{1+\omega_{\mathrm{c}}^2\tau_{\mathrm{rc}}^2} - \varepsilon\left(\frac{\omega_{\mathrm{c}} L_{\mathrm{dyn}}}{1+\omega_{\mathrm{c}}^2\tau_{\mathrm{rc}}^2} + \frac{\omega_{\mathrm{c}}\tau_{\mathrm{m}} 3p^2\psi_{\mathrm{R0}}^2}{2b\left(1+\omega_{\mathrm{c}}^2\tau_{\mathrm{m}}^2\right)}\right)\right]\frac{I_{\mathrm{cd}}^{\varepsilon}}{\sqrt{2}}. \tag{A.35}$$

Since in practice $\omega_{\mathrm{c}}^2\tau^2 \gg 1$, where τ is used for all the time constants in (A.34), the error signal can finally be approximated as

$$F_{\varepsilon} \approx \left[\hat{\omega}_{\mathrm{m}0} \hat{R}_{\mathrm{Rc}} - \omega_{\mathrm{m}0} R_{\mathrm{Rc}} - \varepsilon \left(\frac{R_{\mathrm{Rc}}^2}{L_{\mathrm{dyn}}} + \frac{3p^2 \psi_{\mathrm{R}0}^2}{2J} \right) \right] \frac{I_{\mathrm{cd}}^{\varepsilon}}{\sqrt{2}\omega_{\mathrm{c}}} . \tag{A.36}$$

The first term inside the brackets in (A.36) is due to the second term inside the brackets in (A.33). The term is meant to cancel the middle term in (A.36), which in turn originates from the back-emf response due to a change in the flux amplitude in (A.18).